

## APPENDIX E SITE-SPECIFIC PROBABILISTIC SEISMIC HAZARD ANALYSIS

### E-1. Introduction

*a. Purpose.* The purpose of this appendix is to describe details of the methodology used in probabilistic seismic hazard analysis (PSHA) to develop site-specific response spectra. More general aspects of the site-specific approach are presented in Chapter 3. In paragraph E-2, the formulation of the basic probabilistic model is described. Paragraph E-3 discusses the incorporation of uncertainty in PSHA. Paragraph E-4 describes the results of a PSHA and how they can be analyzed to determine the dominant contributors to the seismic hazard and sources of uncertainty. In paragraph E-5, two examples of applications of PSHA to develop site-specific response spectra are presented.

### E-2. Mathematical Formulation of the Basic Seismic Hazard Model.

#### *a. General Formulation.*

(1) Formulation for probability of exceedance. The methodology used to conduct PSHA was initially developed by Cornell (1968). The formulation of the basic seismic hazard model is summarized herein. Additional discussion and guidance for conducting a PSHA is described in several publications, including National Research Council (1988), Earthquake Engineering Research Institute (1989), and Ferritto (1994, 1997). Using a Poisson probability model, the probability of exceedance,  $p_z(z)$ , of a ground motion level,  $z$ , in an exposure time or design time period,  $t$ , at a site is related to the annual frequency (or rate) of ground motion exceedance at the site,  $v(z)$ , by:

$$p_z(z) = 1 - e^{-(v(z) \cdot t)} \quad (\text{E-1})$$

A PSHA is carried out to obtain  $v(z)$  and  $p_z(z)$  can then be obtained using Equation E-1. The return period (RP) for ground motion exceedance at a site is equal to the reciprocal of  $v(z)$ . The results of a PSHA are, in practice, expressed in terms of one or more of the parameters,  $p_z(z)$ ,  $v(z)$ , and RP. Note that when  $(v(z) \times t)$  is small (approximately  $\leq 0.1$ )  $p_z(z)$  is approximately equal to  $(v(z) \times t)$ . For larger values of  $(v(z) \times t)$ ,  $p_z(z)$  is less than  $(v(z) \times t)$ .

(2) Formulation for frequency of exceedance. The annual frequency of ground motion exceedance,  $v(z)$ , is evaluated using the following expression:

$$n(z) = \sum_{n=1}^N \sum_{m_i=m^o}^{m_i=m^u} I_n(m_i) \sum_{r_j=r_{\min}}^{r_j=r_{\max}} P_n(R=r_j | m_i) \times P(Z > z | m_i, r_j) \quad (\text{E-2})$$

in which

$I_n(m_i)$  = the annual frequency of occurrence of earthquakes on seismic source  $n$  in a magnitude interval centered at  $m_i$ .  $m_i$  is above a minimum size of engineering significance,  $m^o$ , and below the maximum event size,  $m^u$ .

$P_n(R=r_j | m_i)$  = the probability of an earthquake of magnitude  $m_i$  on source  $n$  occurring at a certain distance  $r_j$  from the site

$P(Z > z | m_i, r_j)$  = the probability that ground motion level  $z$  will be exceeded, given an earthquake of magnitude  $m_i$  at distance  $r_j$  from the site

Thus, for a given source, the annual frequency or rate of exceeding a certain ground motion level at the site is obtained by summing over all magnitudes (the second summation of Equation E-2) and source-to-site distances (the last summation of Equation E-2) for that source. Then, the total rate of ground motion exceedance at the site,  $v(z)$ , is obtained by adding the rates for all the sources (the first summation of Equation E-2). The components of equation E-2 are discussed in paragraphs b, c, and d below.

*b. Frequency of Occurrence of Earthquakes.* The incremental rate of earthquakes occurrence  $I_n(m_i)$  is obtained from earthquake recurrence relationships. Two recurrence models are typically used in PSHA, the truncated exponential model and the characteristic earthquake recurrence model. These two recurrence models are also discussed in paragraph 3-4e(3)(b) of Chapter 3. For convenience, the subscript  $n$  for the source region is eliminated in the following paragraphs.

(1) The truncated exponential model of Cornell and Vanmarcke (1969) represents the truncation of the Gutenberg-Richter (1954) earthquake frequency law at a finite upper bound magnitude  $m^u$ . The cumulative form, which expresses the rate of occurrence of earthquakes equal to or greater than a certain magnitude  $m$ , is specified by

$$N(m) = N(m^o) \frac{e^{-b(m-m^o)} - e^{-b(m^U-m^o)}}{1.0 - e^{-b(m^U-m^o)}}, \text{ for } m^o \leq m \leq m^U \quad (\text{E-3})$$

where  $\mathbf{b} = b \ln(10)$  and  $b$  is the  $b$ -value of the Gutenberg-Richter frequency law. Parameters  $\mathbf{b}$  and  $N(m^o)$  are estimated by fitting the recurrence relationship E-3 to the observed recurrence rates obtained from a catalog of historic seismicity. These parameters can be further constrained by the geological slip rate, if it is available. An example of such a truncated exponential recurrence relationship is given on the upper left of Figure E-1. The incremental recurrence rate  $I(m_i)$  is obtained by discretizing the cumulative recurrence curves into narrow magnitude intervals as illustrated in the lower left of Figure E-1.

(2) The characteristic earthquake recurrence model is based on the hypothesized fault behavior that individual fault and fault segments tend to generate same-size or characteristic earthquakes (Schwartz and Coppersmith, 1984; Youngs and Coppersmith, 1985a). "Same-size" usually means within about one-half magnitude unit. There are two implementations of the characteristic earthquake model that are commonly used in PSHA. In the characteristic earthquake recurrence model implemented by Youngs and Coppersmith (1985a), the maximum magnitude  $m^v$  is taken to be the expected magnitude for the characteristic event, with individual events uniformly distributed in the range of  $m^v \pm 3$  magnitude units, representing random variability in individual "maximum" ruptures. The cumulative form of the earthquake recurrence relationship thus becomes

$$\begin{aligned} N(m) &= N^e \frac{10^{-b(m-m^o)} - 10^{-b(m^U - \frac{1}{4} - m^o)}}{1 - 10^{-b(m^U - \frac{1}{4} - m^o)}} + N^c, \\ &\text{for } m^o \leq m < m^U - \frac{1}{4} \\ &= N^c \frac{m^U + \frac{1}{4} - m}{\frac{1}{2}}, \quad \text{for } m^U - \frac{1}{4} \leq m \leq m^U + \frac{1}{4} \end{aligned} \quad (\text{E-4})$$

where the terms  $N^e$  and  $N^c$  represent the rate of exponential and characteristic events, respectively.  $N^e$  and  $N^c$  are specified by the slip rate of the individual fault using the formulation of Youngs and Coppersmith (1985a).

$$\begin{aligned} N^e &= \frac{\dot{M}_o^T (1 - 10^{-b(m^U - \frac{1}{4} - m^o)})}{M_o^U 10^{-b(m^U - \frac{1}{4} - m^o)} \left[ \frac{b10^{-\frac{c}{2}}}{c-b} + \frac{b10^b(1 - 10^{-\frac{c}{2}})}{c} \right]} \\ N^c &= \frac{\frac{1}{2} b \ln(10) N^e 10^{-b(m^U - \frac{1}{4} - m^o - 1)}}{1 - 10^{-b(m^U - \frac{1}{4} - m^o)}} \end{aligned} \quad (\text{E-5})$$

where  $\dot{M}_o^T$  is the rate of seismic moment release along a fault and  $M_o^U$  is the seismic moment for the upper limit event  $m^v + 3$ .  $\dot{M}_o^T$  is estimated by  $\mu A_f S$ , where  $\mu$  is the shear modulus of fault zone rock (assumed to be  $3 \cdot 10^{11}$  dyne/cm<sup>2</sup>),  $A_f$  is the total fault surface area,  $S$  is the slip rate. An example of such a characteristic recurrence relationship is given on the upper right of Figure E-1 and the incremental rate  $I(m_i)$  is given on the lower right.

(3) In another implementation of the characteristic earthquake model (Wesnousky, 1986), no allowance is made for the occurrence of events of sizes other than the characteristic size. The characteristic size ( $m^c$ ) is proportional to fault length and can be determined using relations such as those in Wells and Coppersmith (1994). The recurrence rate for this characteristic size earthquake is thus

$$I(m^c) = \frac{\dot{M}_o^T}{M_o^c} \quad (\text{E-6})$$

where  $M_o^c$  is the seismic moment of the characteristic size earthquake  $m^c$ . This version of the characteristic earthquake recurrence model (called the maximum magnitude model by Wesnousky, 1986) has been used by USGS (1996) and others in PSHAs (e.g. Ferritto, 1994).

*c. Distance Probability Distribution.* The distance probability distribution,  $P(R=r_j/m_i)$ , depends on the geometry of earthquake sources and their distance from the site; an assumption is usually made that earthquakes occur with equal likelihood on different parts of a source. The function  $P(R=r_j/m_i)$  also should incorporate the magnitude-dependence of earthquake rupture size; larger-magnitude earthquakes have larger rupture areas, and thus have higher probability of releasing energy closer to a site than smaller-magnitude earthquakes on the same source. An example of probability distributions for the closest distance to an earthquake source is shown in Figure E-2. In this particular example, the source (fault) is characterized as a line source and the probability distributions are based on

the formulations presented by Der Kiureghian and Ang (1977). Figure E-2 (diagram a) illustrates the probability distributions for a fault rupture length of 5 km (3.1 miles); Figure E-2 (diagram b) illustrates the probability distributions for a fault rupture length of 25 km (15.5 miles). The longer rupture length corresponds to a larger magnitude. The figure shows the distributions for both the probability of the closest distance to the fault rupture,  $R$ , being less than a certain value,  $P(R < r_j/m_i)$  and the probability of earthquakes occurring at a certain distance

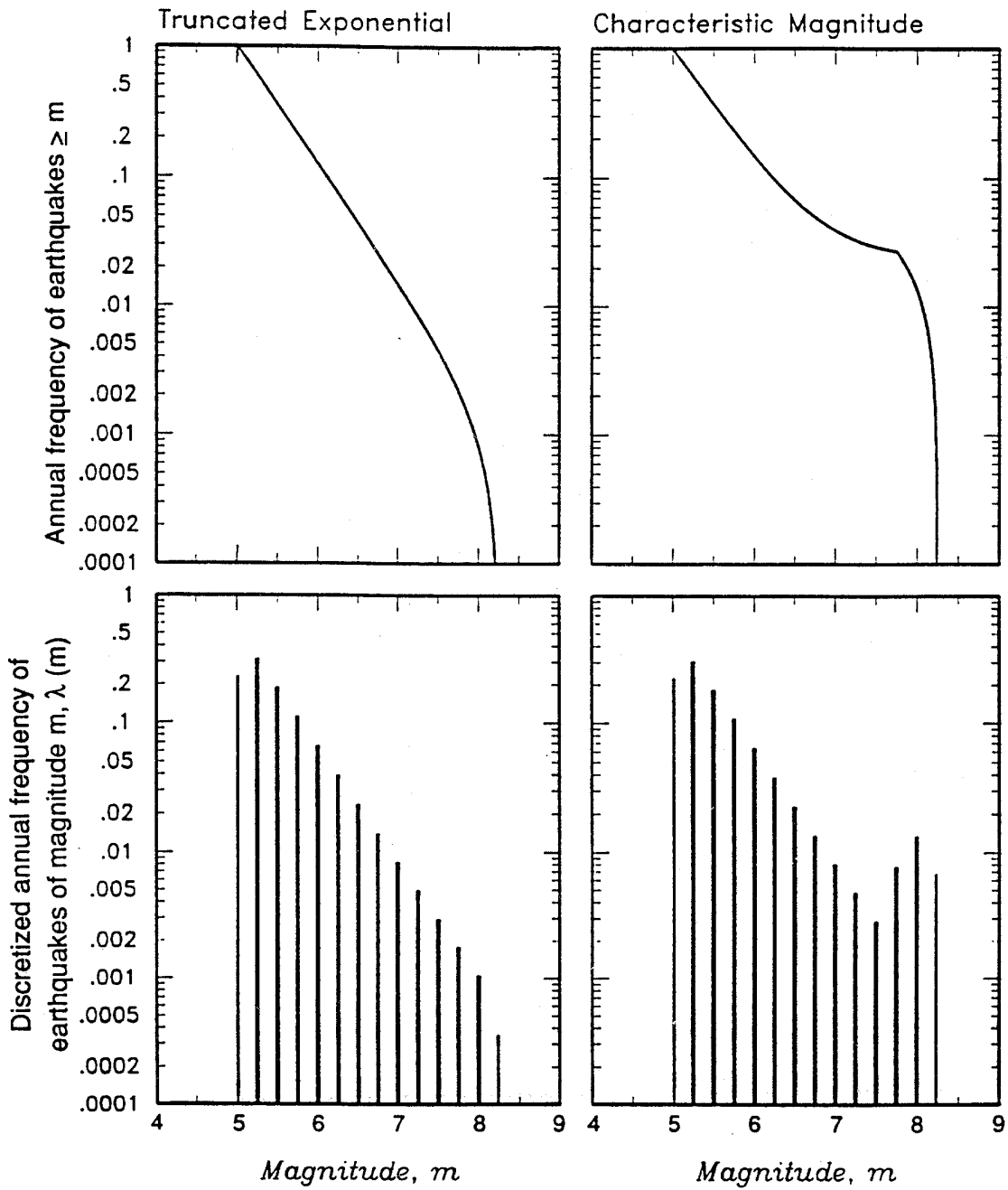


Figure E-1 Typical earthquake recurrence curves and discretized occurrence rates.

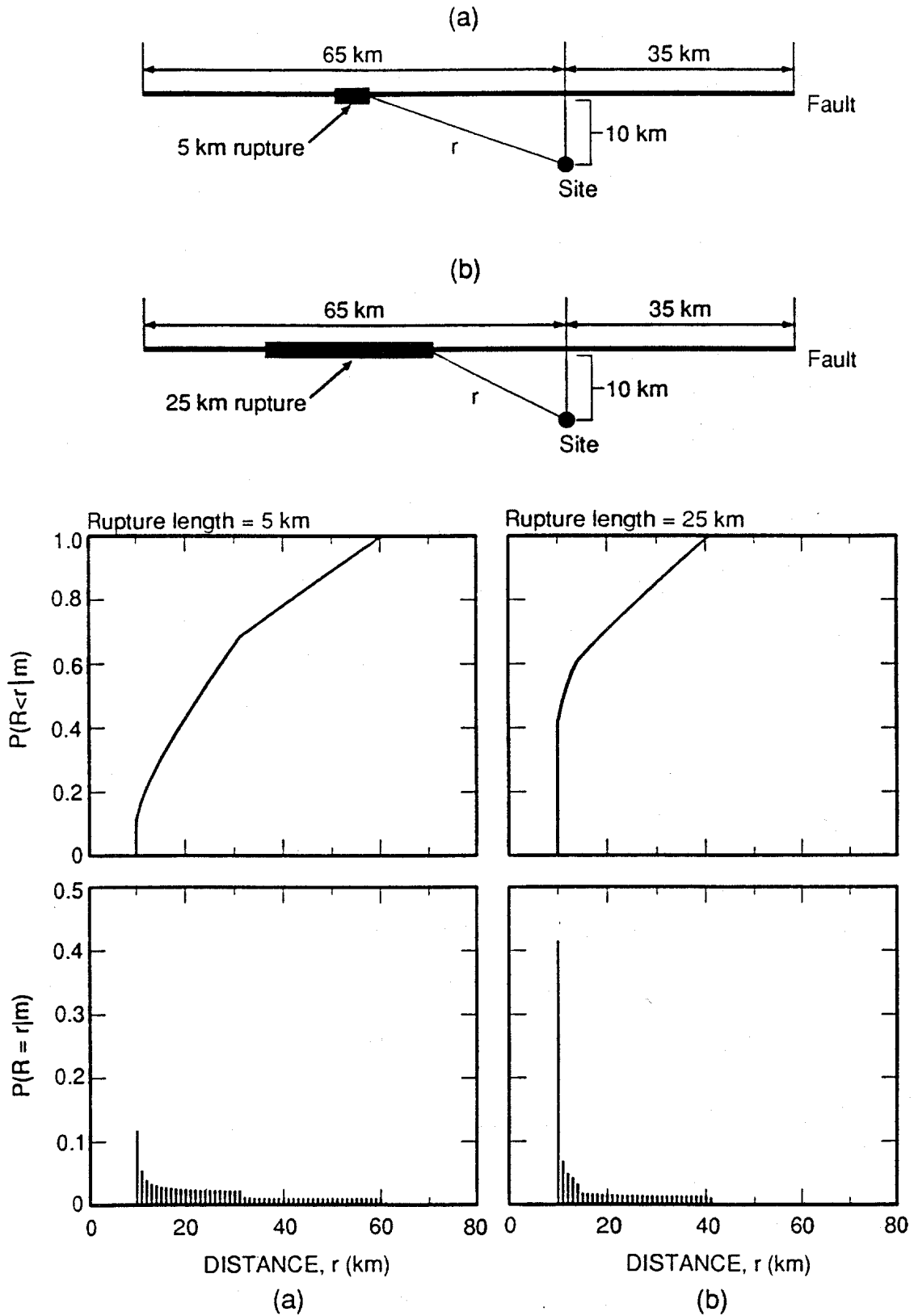


Figure E-2 Illustration of distance probability distribution.

( $P(R=r_j/m_i)$ ), which is obtained by discretizing the curves for  $P(R < r_j/m_i)$ . The higher probability for earthquakes to occur at closer distances for longer rupture lengths (larger magnitudes) can be noted by comparing Figure E-2 (diagram b) with E-2 (diagram a). Note that the distance to the earthquake rupture must be expressed in terms of the same definition of distance as used in the ground motion attenuation relationships. Typically, some form of closest distance to rupture definition is used for attenuation relationships (variations in this definition include: closest distance to rupture, closest distance to rupture of the seismogenic zone (at some depth below ground surface), closest horizontal distance to surface projection of rupture, etc.).

#### *d. Ground Motion Exceedance Probability*

*Distribution.* The conditional probability of exceeding a ground motion level for a certain earthquake magnitude and distance,  $P(Z > z/m_i, r_j)$ , is determined from the ground motion attenuation relationships selected for the site. As noted in paragraph 3-4f of Chapter 3 and illustrated in Figure 3-11, attenuation relationships are available for response spectral values as well as for peak ground acceleration. Uncertainty in the median attenuation curves is incorporated, as illustrated in Figures 3-3, 3-4 and 3-11. The function  $P(Z > z/m_i, r_j)$  is usually evaluated assuming that ground motion values are log-normally distributed about the median value; the calculation of this function is illustrated in Figure E-3.

### **E-3. Treatment of Modeling and Parameter Uncertainties in PSHA.**

The basic probability formulations in Equations E-1 and E-2 incorporate the randomness of the physical process of earthquake generation and seismic wave propagation. Although these formulations incorporate the inherent uncertainty due to randomness, they do not incorporate additional sources of uncertainty that may be associated with the choice of particular models or model parameters. For example, there could be uncertainty as to which ground motion attenuation relationship is most applicable to a site, uncertainty as to whether an exponential or characteristic earthquake recurrence model is most applicable, uncertainty in the geometry of earthquake sources, uncertainty in the values of maximum earthquake magnitude, uncertainty in earthquake recurrence parameters, etc. In a deterministic analysis, these uncertainties, which are termed epistemic uncertainties, are usually treated by applying conservatism in selecting design earthquakes and estimating ground motions. In PSHA, these uncertainties can be directly modeled within the analysis framework to provide an assessment of the uncertainty in the result. The technique of “logic trees” has

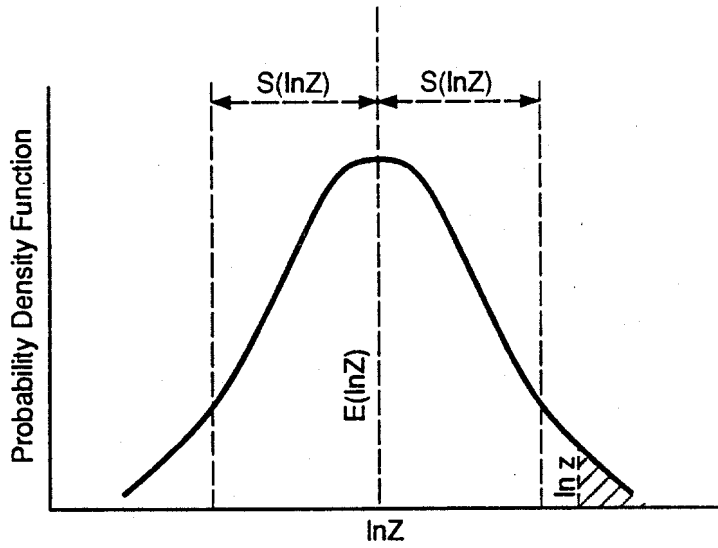
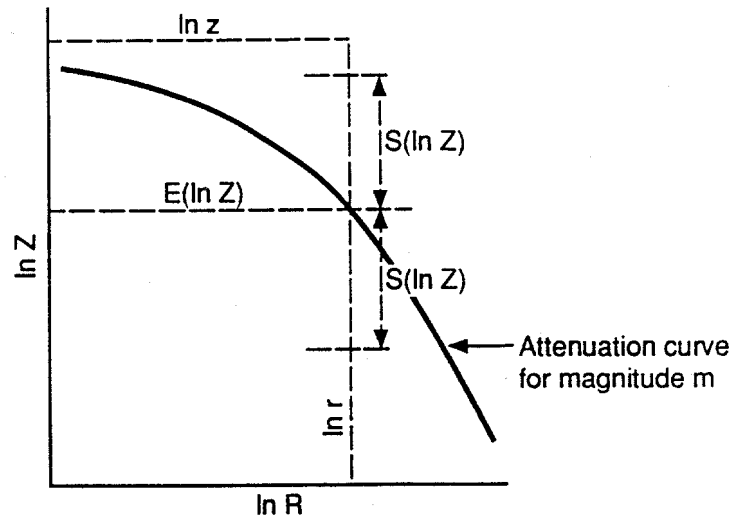
been widely used to incorporate scientific uncertainty in a PSHA (Kulkarni et al., 1984; Youngs et al., 1985; Coppersmith and Youngs, 1986; National Research Council, 1988; SSHAC, 1997). Figure E-4 shows an example of a logic tree used in a PSHA. Although only a few branches of the logic tree are shown, there may be many thousands of branches in the tree. Each path through the tree to an end branch (on the right-hand side of the Figure E-4) defines a set of parameters that are used to conduct a basic seismic hazard analysis for that path and end branch using Equation E-2. Basic hazard analyses are carried out for each path. Each path also has an associated probability or weight that is determined by the product of the relative probabilities or weights assigned to the various models and parameters along the path. (The relative probabilities or weights of the alternative models and parameters are illustrated by the numbers in parentheses in Figure E-4.) The basic hazard analysis results for all the paths are combined using the associated weights to arrive at best estimates (mean or median values) for the frequencies of exceedance of ground motions as well as uncertainty bands for the estimates. Through the approach of incorporating scientific uncertainty, PSHA incorporates the alternative hypotheses and data interpretations that may significantly affect the computed results. The display and analysis of uncertainty in the seismic hazard is discussed in the following section.

### **E-4. Analysis Results.**

*a. Basic Results.* The basic results of a PSHA are seismic hazard curves (curves of the amplitude of a ground motion parameter at a site vs. frequency of exceedance). An example of the typical form of results is illustrated in Figure E-5 for the parameter of peak ground acceleration. A distribution of seismic hazard curves ranging from the 5<sup>th</sup> to the 95<sup>th</sup> percentile is shown. This distribution results from the incorporation of scientific uncertainty in the PSHA through the use of logic trees as discussed above. Typically, the mean curve or median (50<sup>th</sup> percentile) curve is used to obtain design parameters, while the various percentiles of the distribution are a measure of the uncertainty in the result. Note in Figure E-5 that the mean curve lies above the median curve. This result is typical of seismic hazard analysis. In general, the mean curve rather than the median curve is the preferred measure of the hazard results. The use of hazard curve results to develop response spectra is described in paragraph 3-4h of Chapter 3.

*b. Analysis of Contribution to the Seismic Hazard.* A hazard curve incorporates contributions from different earthquake sources, magnitudes, and source-to-site distances. The results can be analyzed to determine the

major contributions to the hazard. For example,  
contributions of different earthquake sources to the mean



$$P(Z > z | m, r) = 1 - F_U \left( \frac{\ln z - E(\ln Z | m, r)}{S(\ln Z | m, r)} \right)$$

#### EXPLANATION

$E(\ln Z)$  is the expected value of  $\ln Z$

$S(\ln Z)$  is the standard deviation of the estimate of  $\ln Z$

$F_U$  is cumulative distribution function of a unit normal variable

Figure E-3 Ground motion estimation conditional probability function.

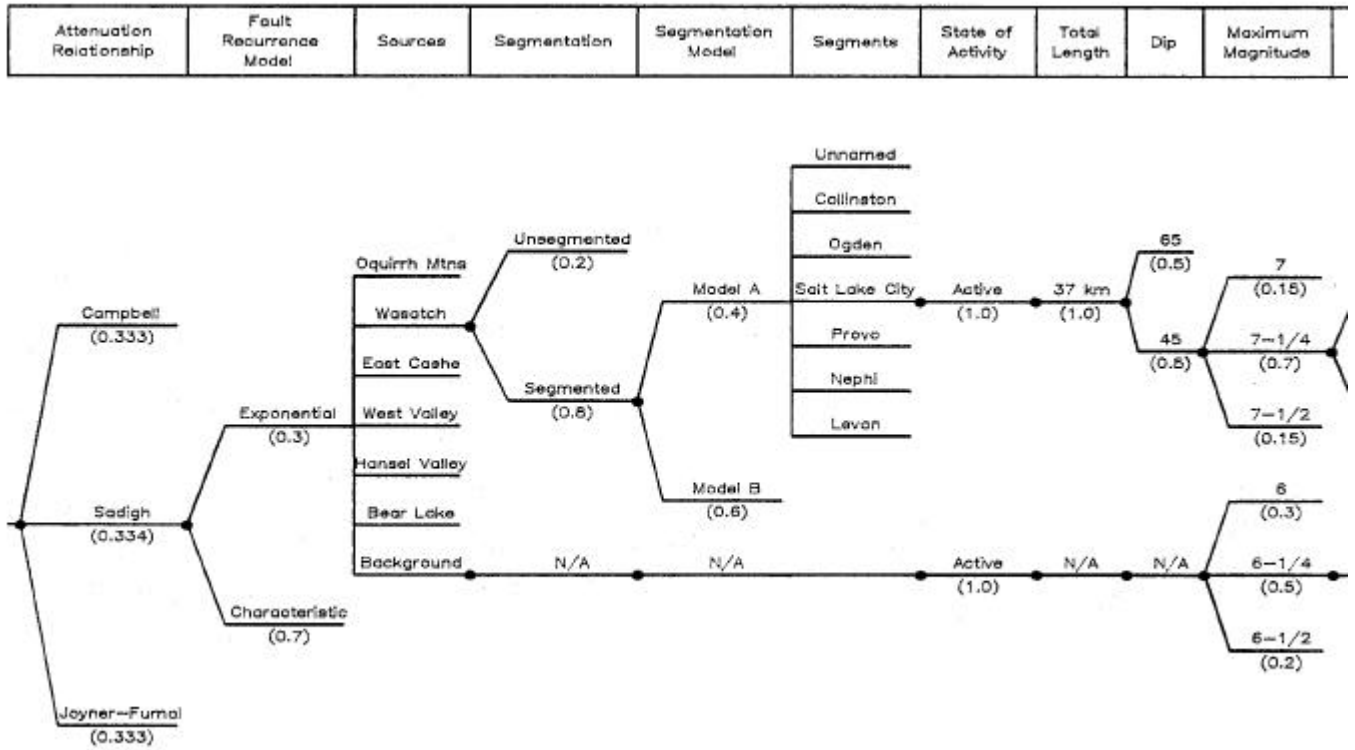


Figure E-4 Example logic tree for characterizing uncertainty in seismic hazard input (Youngs et al., 1988)

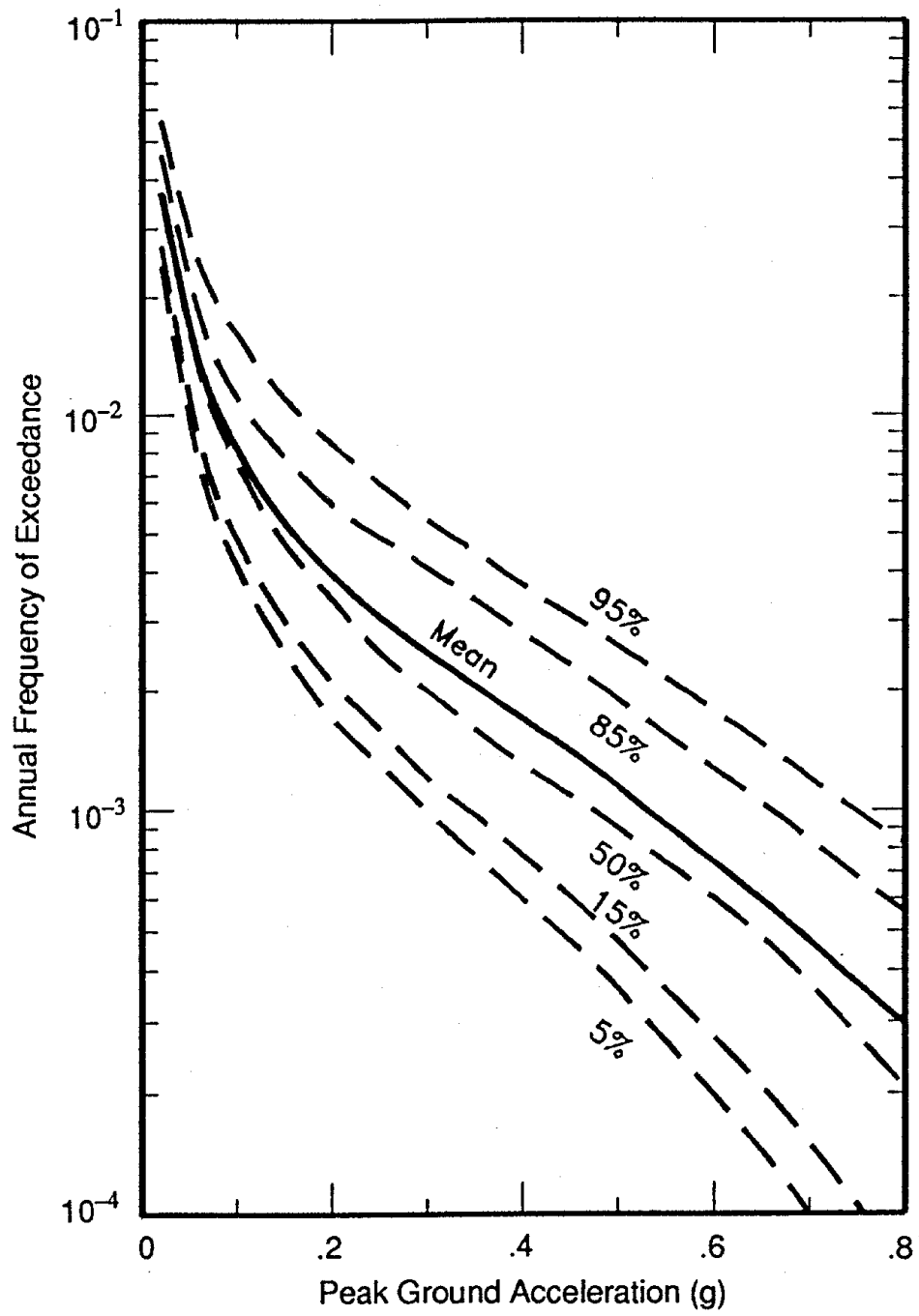


Figure E-5 Example of distribution of seismic hazard results.

hazard curves for three ground motion parameters (peak ground acceleration and response spectral values at periods of vibration of 0.3 and 3.0 seconds) at a site are illustrated in Figure E-6. The contributions of different earthquake magnitudes to the seismic hazard at the same site are illustrated in Figure E-7. As shown in the example in Figure E-7, there is increasing contribution to the hazard from large magnitude earthquakes as the response spectral period of vibration increases. This result is typical and reflects the larger influence of magnitude on ground motions at longer periods, as illustrated in the attenuation curves in Figure 3-10 of Chapter 3. Also as shown, the contribution of larger magnitude earthquakes increases as the return period increases (probability level decreases). This result is also typical and reflects the lesser ability of smaller magnitude earthquakes to produce high levels of ground motion. An analysis similar to that shown in Figure E-7 can also be made to identify the dominant distance ranges contributing to the seismic hazard (although the distance contributions may be adequately described by the source contributions in many cases). In cases where site-specific acceleration time histories are required, such analyses of the dominant contributors to the site ground motion hazard are essential to the process of selecting or developing time histories that have appropriate characteristics, including an appropriate duration of strong shaking (duration is strongly correlated with earthquake magnitude).

*c. Analysis of Contributions to Uncertainty in the Seismic Hazard.* The results of a PSHA can also be analyzed to identify those components of the seismic hazard model that primarily contribute to uncertainty in the hazard results, as reflected in the hazard curve distributions such as illustrated in Figure E-5. This uncertainty is due to the alternative models and parameter values incorporated in the logic tree. The analysis of two potential contributors to uncertainty in seismic hazard results is illustrated in Figures E-8 and E-9. In Figure E-8, it can be seen that uncertainty in the choice of ground motion attenuation relationships contributed substantially to the overall uncertainty in seismic hazard (as measured by the 5<sup>th</sup> to 95<sup>th</sup> percentile hazard curve results) for this particular site. In Figure E-9, it can be similarly seen that uncertainty in maximum earthquake magnitude contributed only moderately to the overall uncertainty in seismic hazard for the same site.

## **E-5. Examples of PSHA Usage in Developing Site-Specific Response Spectra.**

*a. Introduction.* In the following two subsections, examples of the application of PSHA in developing site-

specific response spectra are presented. These examples illustrate the characterization of analysis inputs, analysis of the results, and development of equal hazard response spectra. The first example is a relatively high-hazard site in the San Francisco Bay Area in California; the second example is a moderate hazard site in southern Illinois.

### *b. Site in San Francisco Bay Area.*

#### (1) Seismic source characterization.

(a) The site is a rock site located approximately 21 km (13 miles) east of the San Andreas fault and 7 km (4.3 miles) west of the Hayward fault, as shown in Figure E-10. The seismic sources, including discrete faults and area sources, are shown in Figure E-11. The corridors shown around the faults are for the purposes of analyzing the seismicity that is likely associated with the faults.

(b) For each fault, cumulative earthquake recurrence based on seismicity was plotted and compared with earthquake recurrence based on geologic slip rate data for the fault. For the slip-rate-based recurrence assessments, two magnitude distribution models were initially used: exponential model; and characteristic model. Comparisons of recurrence estimated for each model with seismicity were made. Examples of these comparisons for the San Andreas fault and Hayward fault are shown in Figures E-12 and E-13. These comparisons and comparisons for other faults indicate that the characteristic magnitude distribution used in conjunction with fault slip rate data provided recurrence characterizations in good agreement with seismicity data. On the other hand, the exponential magnitude distribution used with the fault slip rate data resulted in recurrence rates that exceeded the rates from seismicity data. From these comparisons and comparisons for the other faults, it was concluded that the fault-specific recurrence was appropriately modeled using the characteristic magnitude distribution model and this model was used for all the fault-specific sources. Recurrence on the area sources was modeled using both: (1) the exponential magnitude distribution and seismicity data; and (2) both the exponential and characteristic magnitude distributions and tectonic data on plate convergence rates in the San Francisco Bay Area. For the entire central Bay Area, a comparison was made between the recurrence predicted by the adopted recurrence models and the observed seismicity. This comparison is shown in Figure E-14 and illustrates good agreement. The faults contribute much more to the regional recurrence than the area sources. Because the fault recurrence is modeled using geologic slip-rate data, the comparison in Figure E-14 is indicative of good agreement between seismicity and

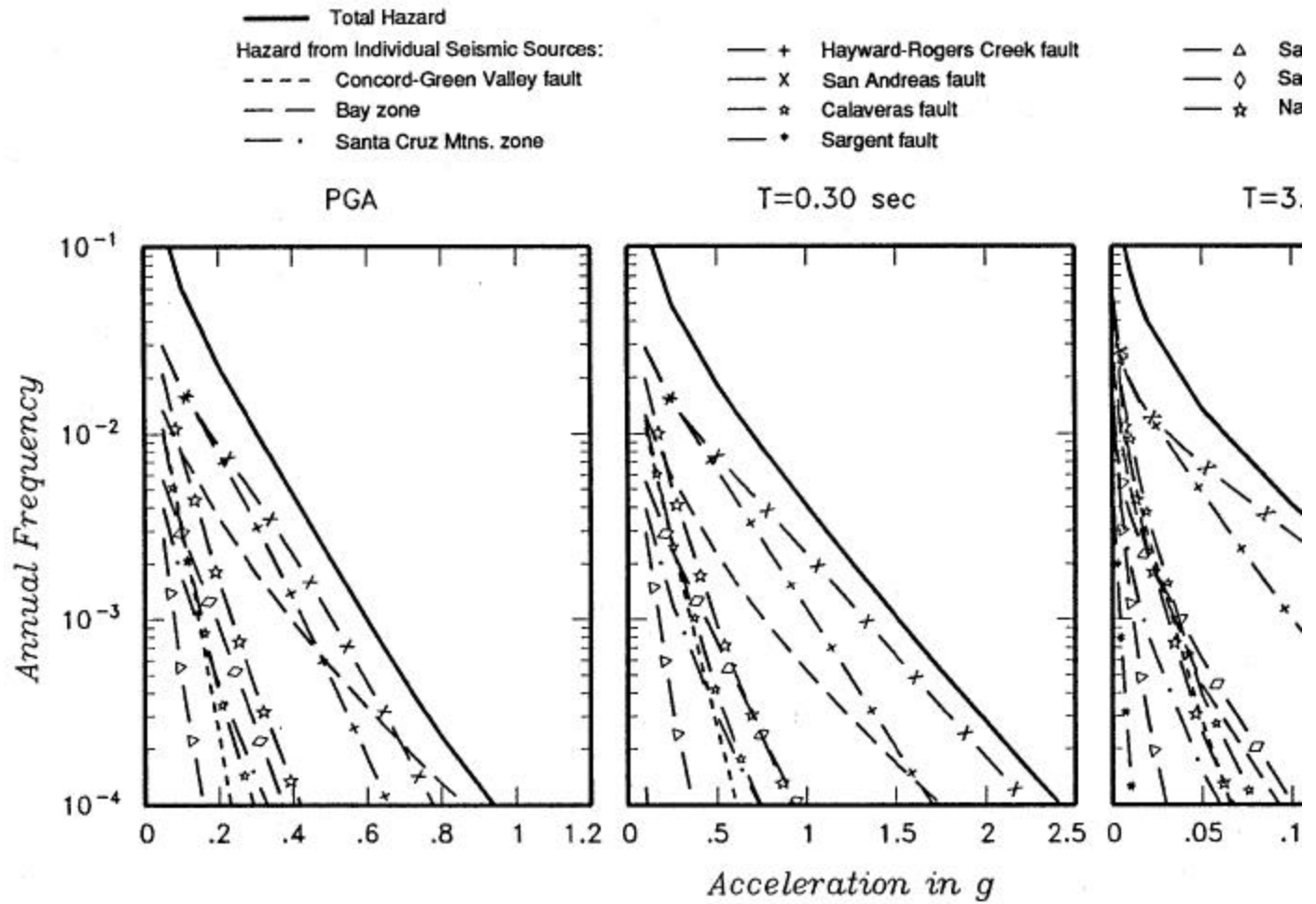


Figure E-6 Example of contributions of various seismic sources to the mean hazard at a site.

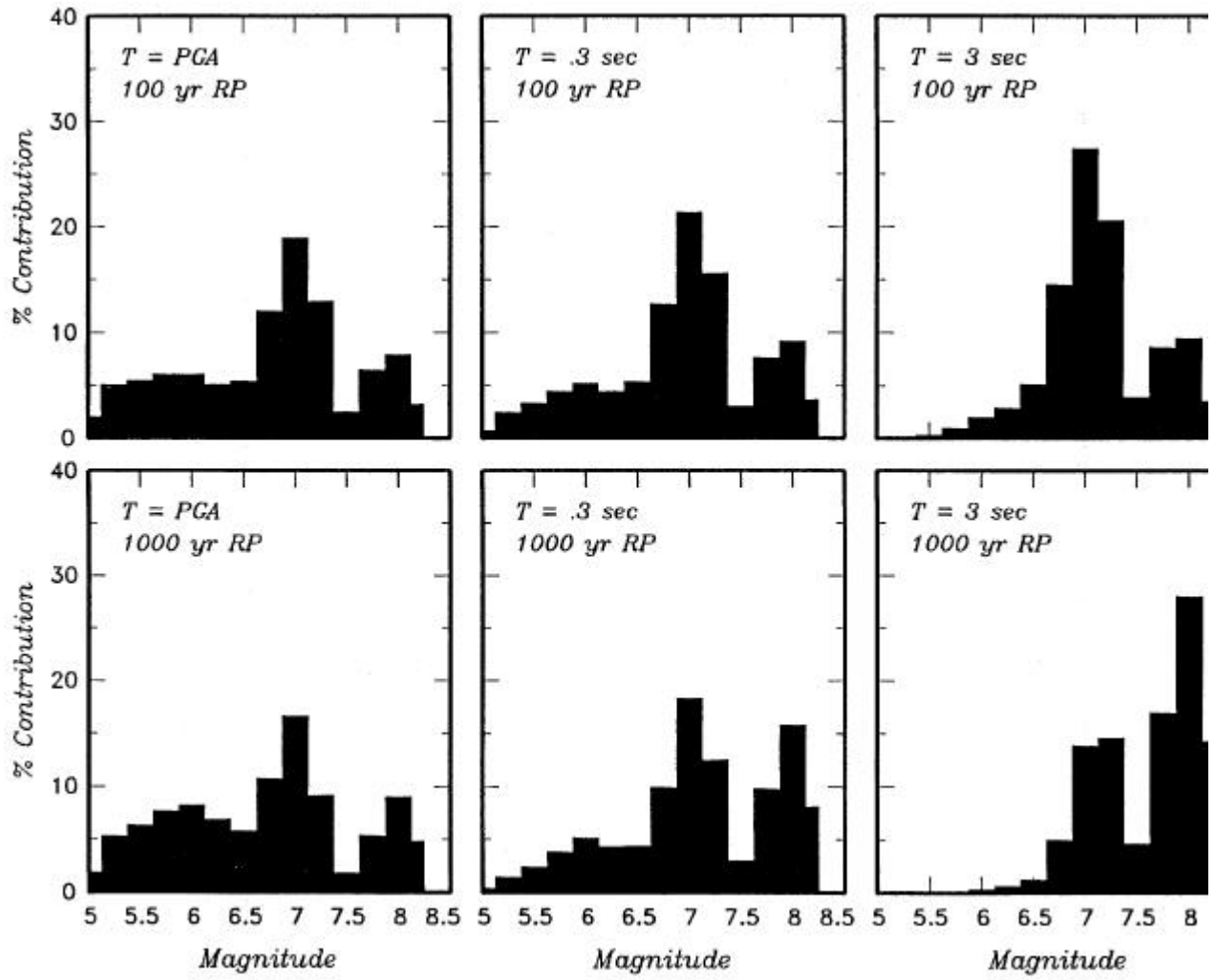


Figure E-7 Example of contributions of events in various magnitude intervals to the hazard for peak acceleration at periods of 0.3 and 3.0 seconds.

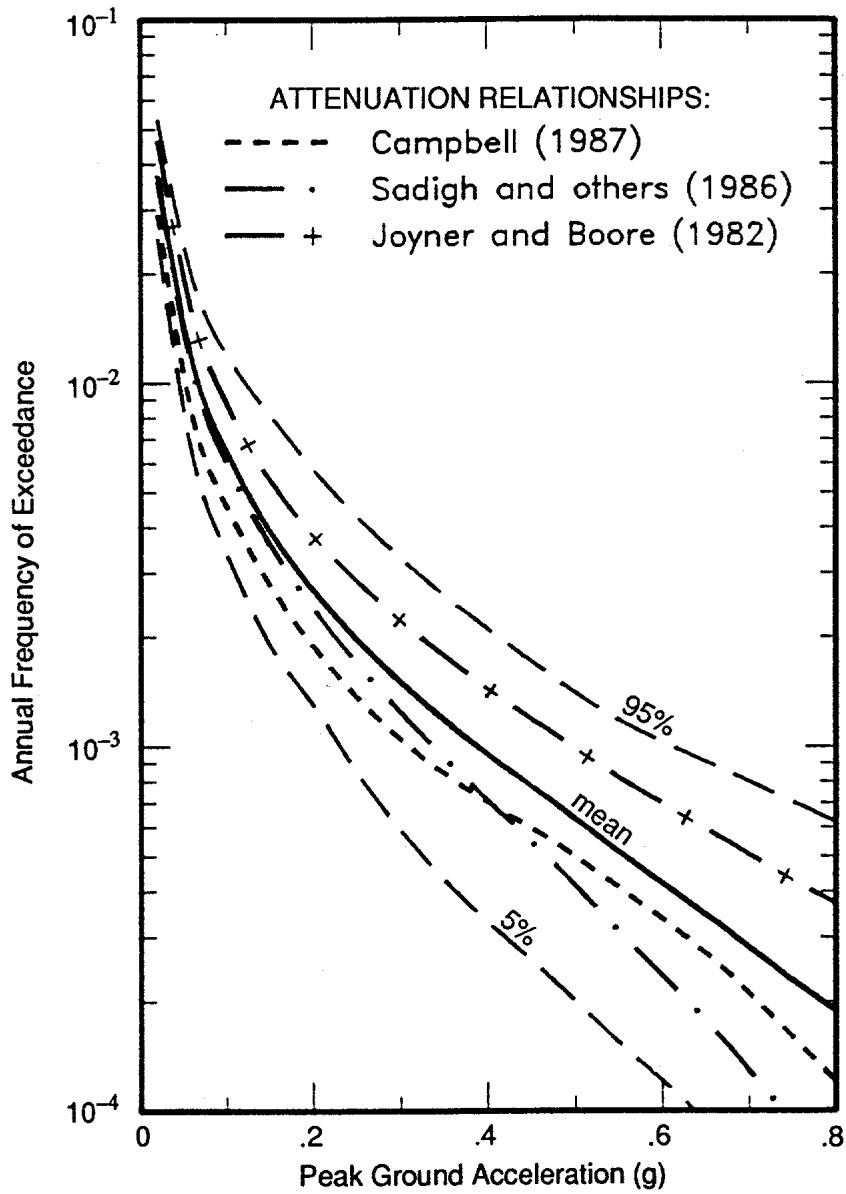


Figure E-8 Example of uncertainty in attenuation contribution to seismic hazard uncertainty.

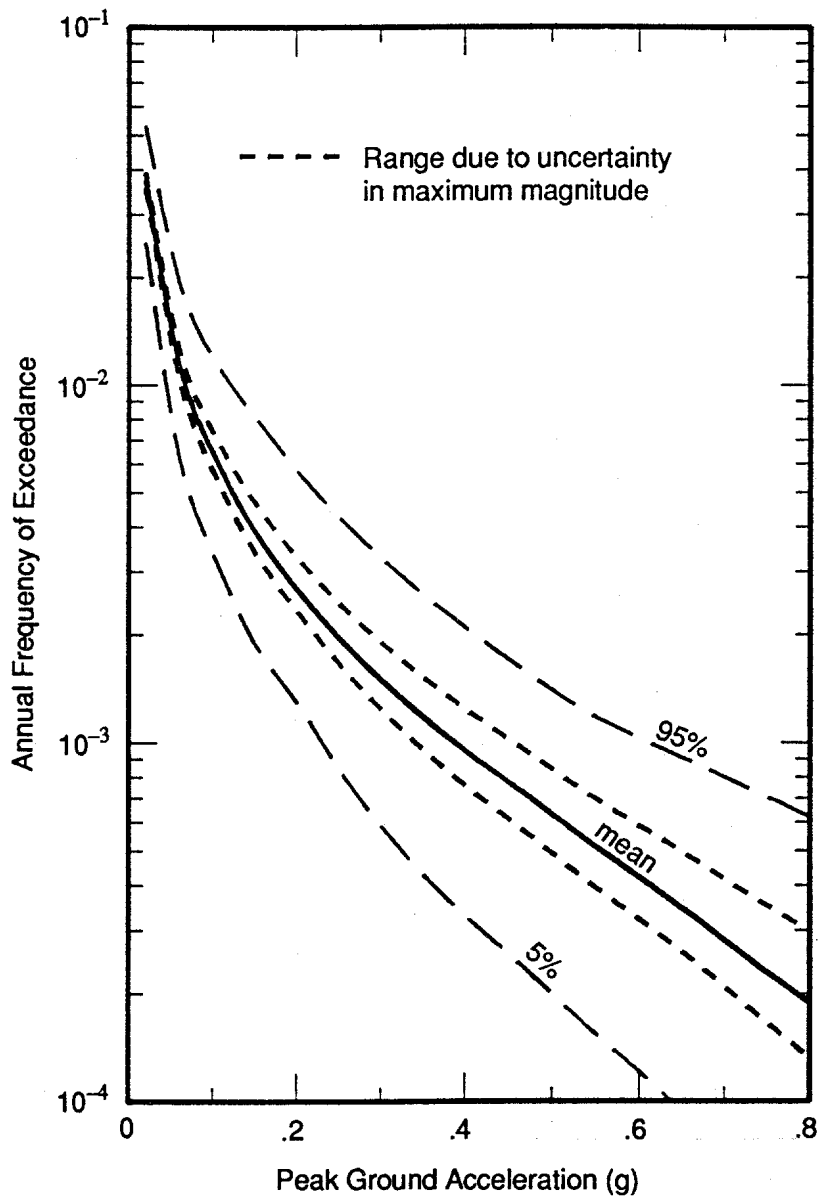


Figure E-9 Example of uncertainty in maximum magnitude contribution to seismic hazard uncertainty.

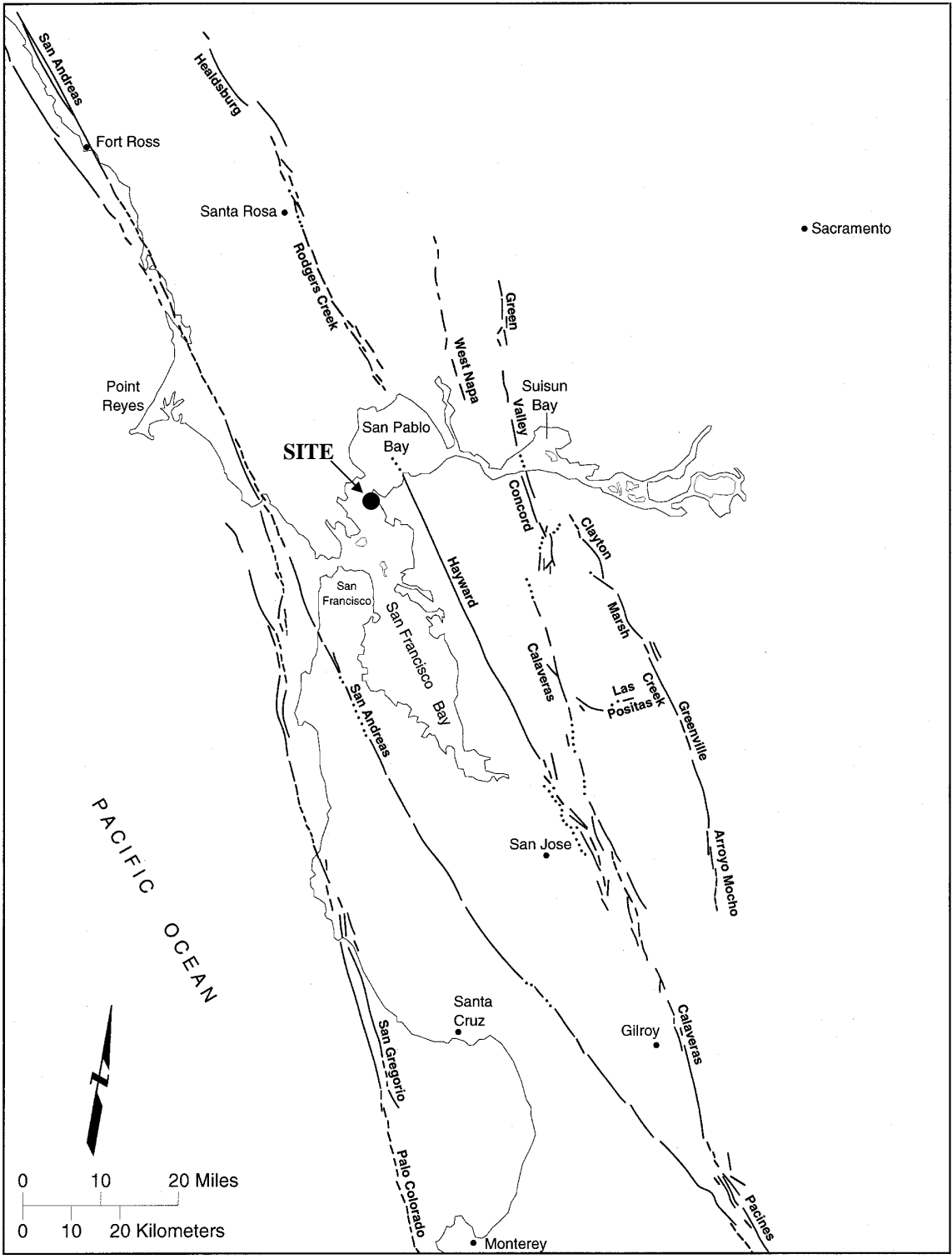


Figure E-10 Regional active fault map, San Francisco Bay area.

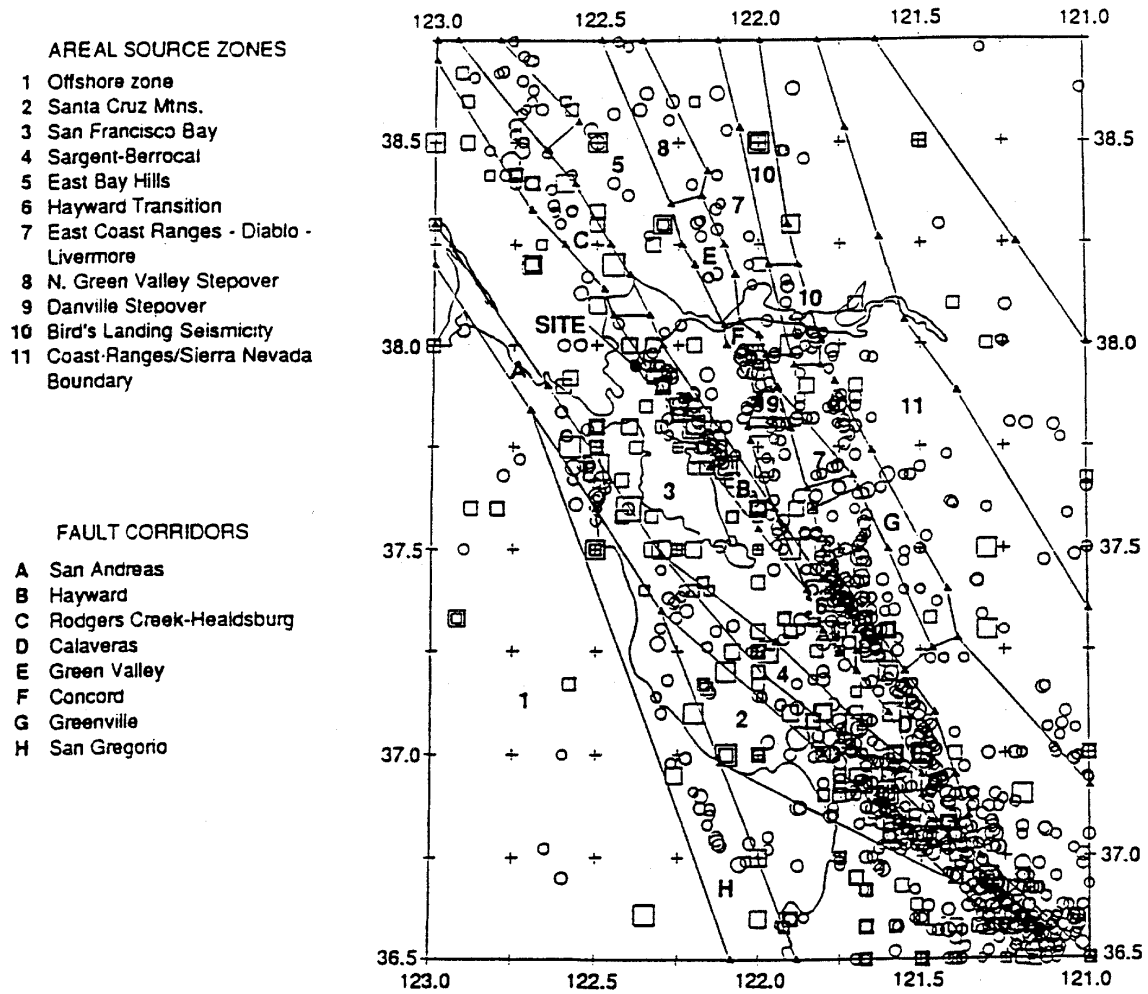


Figure E-11 Map of the San Francisco Bay Area showing independent earthquakes, fault corridors, and areal source zones.

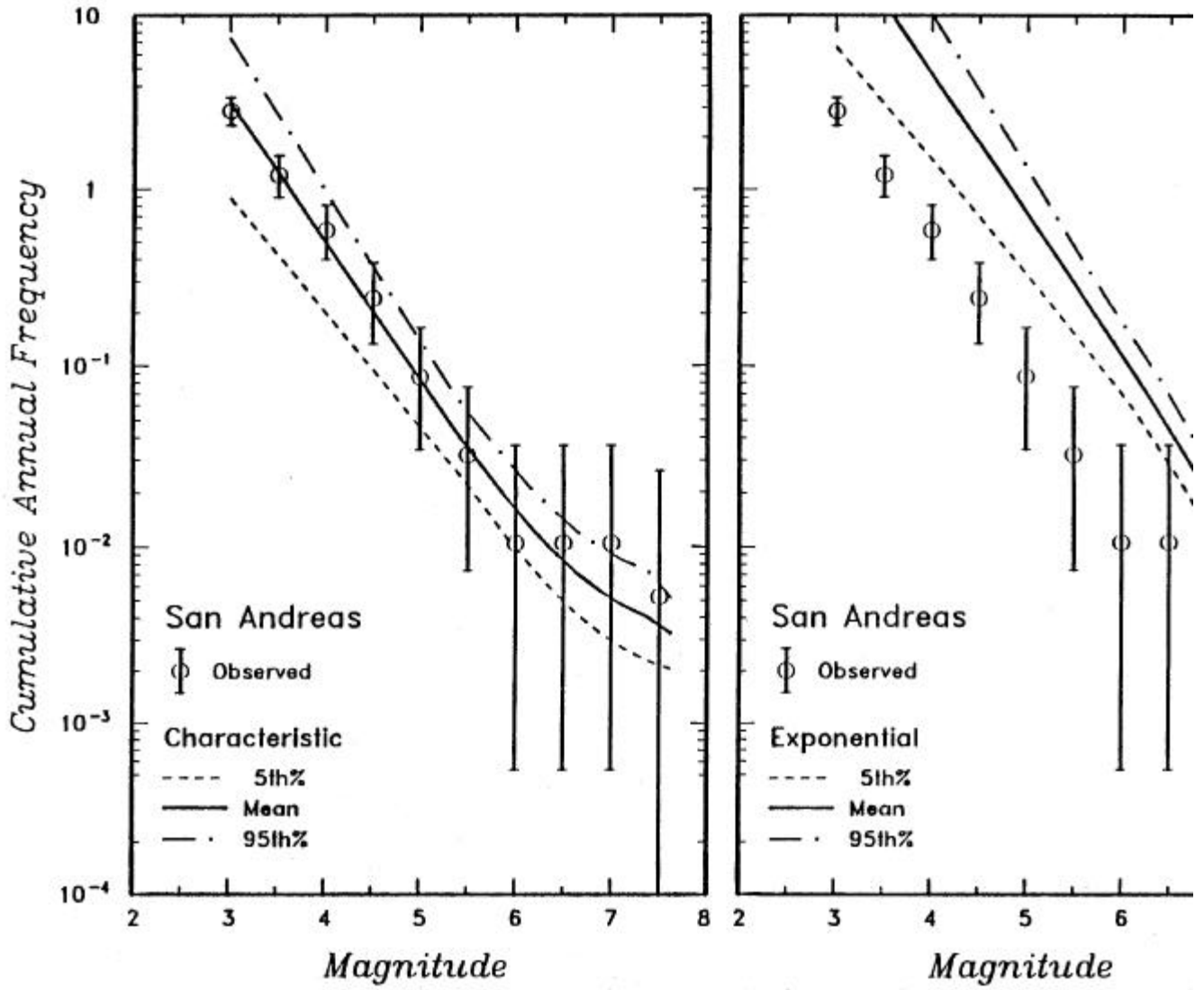


Figure E-12 Comparison of recurrence rates developed from independent seismicity and from fault slip rate fault.

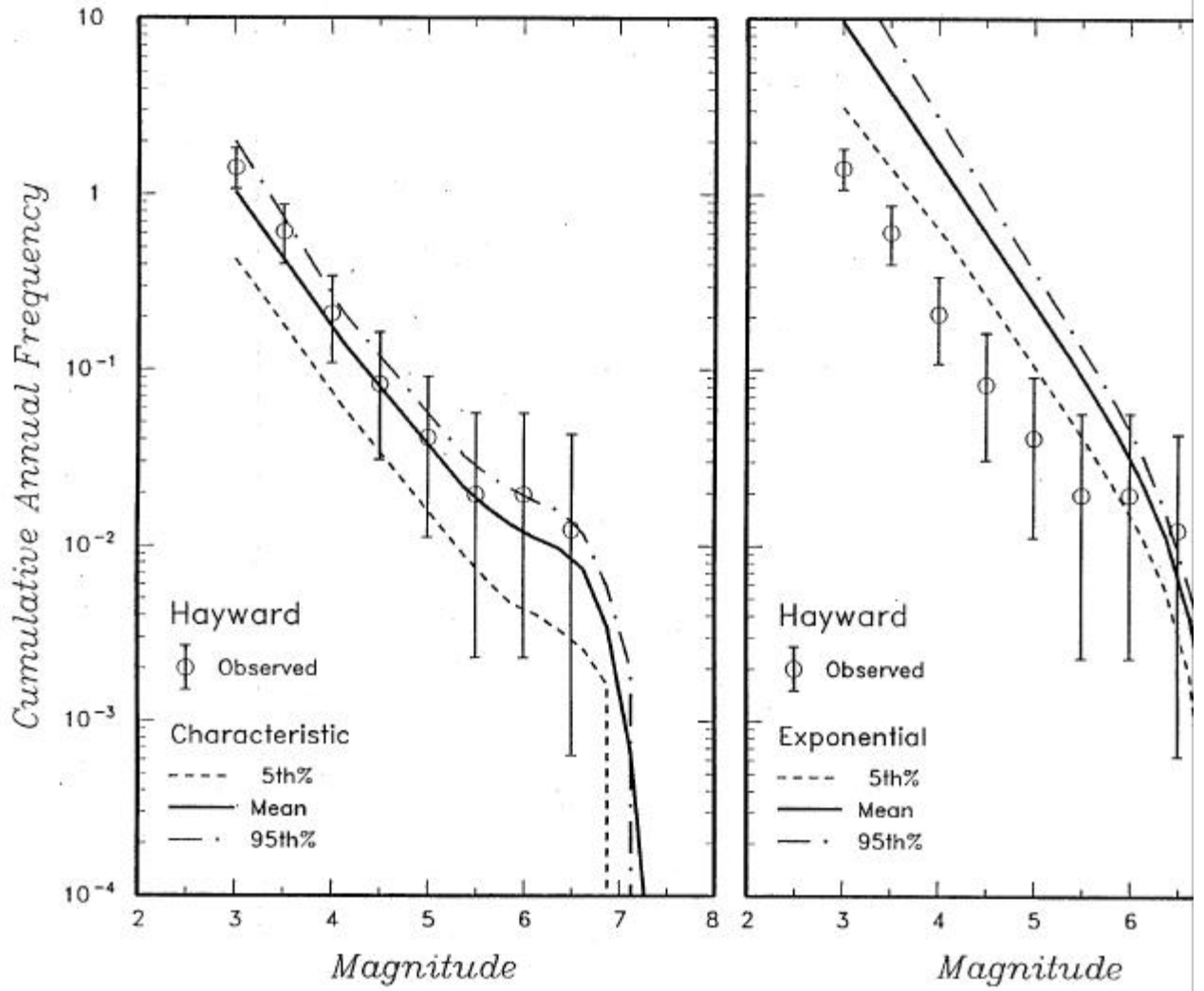


Figure E-13 Comparison of recurrence rates developed from independent seismicity and from fault slip rate

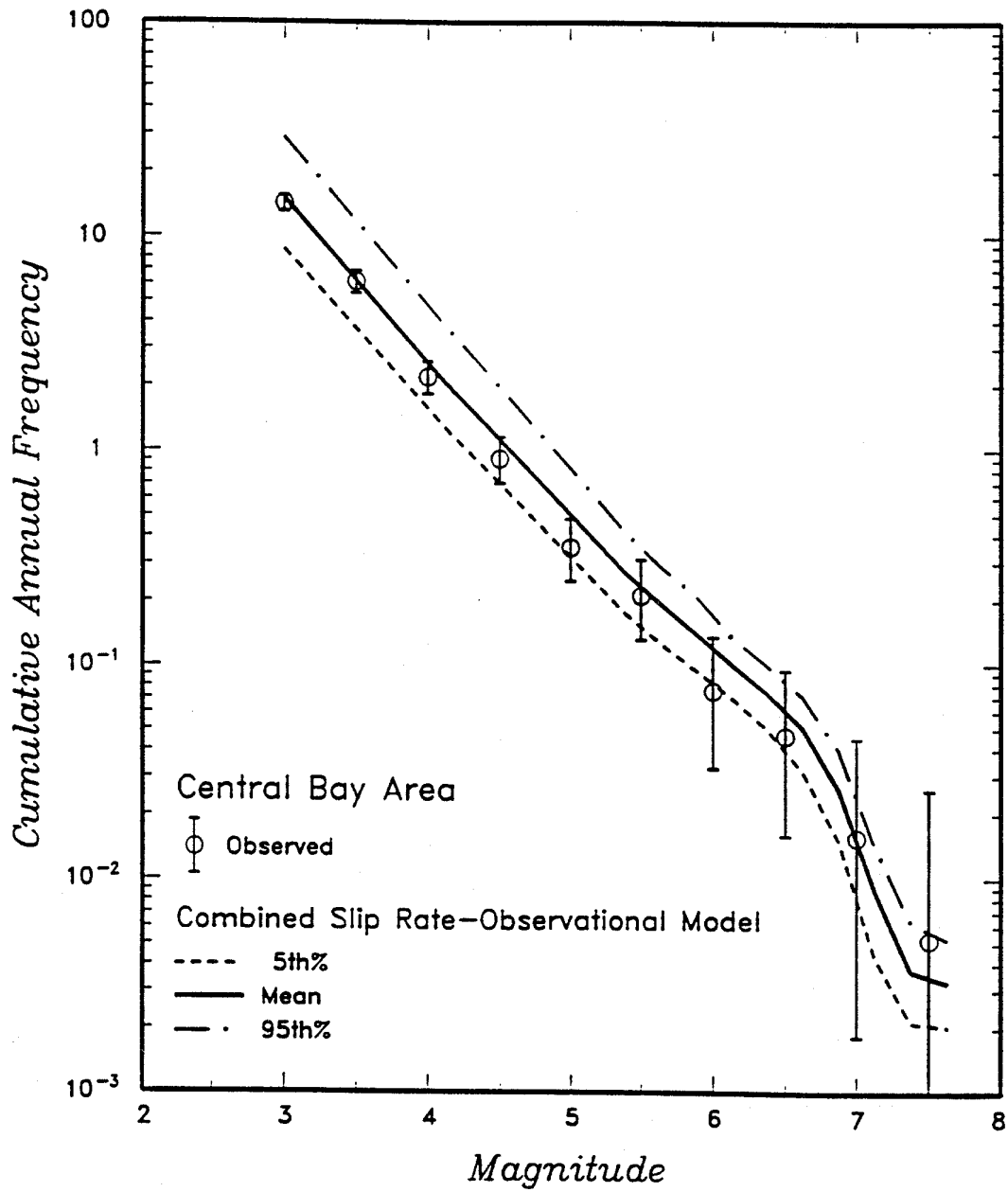


Figure E-14 Comprehensive recurrence model for the Central Bay Area.

geologic data in defining the regional rate of earthquake activity.

(c) Figure E-15 illustrates the generic logic tree for seismic source characterization used for the PSHA. As shown, the study incorporated uncertainty and alternative hypotheses and parameter values for segmentation, maximum rupture length (influencing maximum earthquake magnitude), maximum magnitude estimate correlations, recurrence approach (alternatives of using seismicity data and tectonic convergence rate data for source zones), recurrence rates and b-values, and magnitude distribution model for recurrence assessments (characteristic for faults and characteristic and exponential for area sources).

(2) Ground motion attenuation characterization. Three different sets of rock ground motion attenuation relationships for response spectral acceleration at different periods of vibration (5 % damping) as well as for peak acceleration were utilized. Median values for these relationships (for magnitudes 5, 6, and 7) are illustrated in Figure E-16 for peak acceleration and spectral acceleration at two periods of vibration. Each set of these relationships also has its associated model of uncertainty (dispersion) around the median curves. The dispersion relationships for the preferred model (designated Caltrans, 1991, in Figure E-16 are summarized in Table E-1. (The attenuation model designated Caltrans, 1991, is the relationship of Sadigh et al., 1993). Note that this model predicts increasing dispersion for decreasing magnitude and increasing period of vibration, based on analysis of ground motion data. The three sets of attenuation relationships comprise three additional branches that are added to the logic tree in Figure E-15.

### (3) PSHA Results

(a) Typical results of the PSHA are illustrated in Figure E-17 in terms of the hazard curves obtained for peak acceleration and response spectral acceleration at two periods of vibration. The distribution about the mean hazard curve represents the uncertainty in seismic source characterization and ground motion attenuation characterization modeled in the logic tree.

(b) Figure E-18 shows the contributions of different seismic sources to the hazard (sources are shown in Figures E-10 and E-11). As shown, the Hayward fault, which is closest to the site, dominates the hazard for PGA and spectral values at low periods of vibration, but the San Andreas fault contribution increases with increasing vibrational period (reflecting the potential for larger

magnitude earthquakes on the San Andreas fault than on the Hayward fault and the relatively greater influence of magnitude on long-period motions than short-period motions).

(c) Magnitude contributions to the mean hazard curves are illustrated in Figure E-19. The contributions of higher magnitudes increase both with increasing period of vibration and with increasing return period (RP).

(d) Analyses of two of the components of the seismic hazard model that contribute to the uncertainty in the hazard curves are illustrated in Figures E-20 and E-21. From Figure E-20 it can be seen that much of the uncertainty in the hazard curves is associated with uncertainties as to the appropriate attenuation relationship. The uncertainty in the hazard associated with different models of earthquake recurrence for the San Andreas fault (different segmentation models) (Figure E-21) is small, particularly at lower frequencies of exceedance.

(e) Equal hazard response spectra (expressed in the form of tripartite plots) constructed from the mean hazard results are shown in Figure E-22 for return periods varying from 100 to 2000 years.

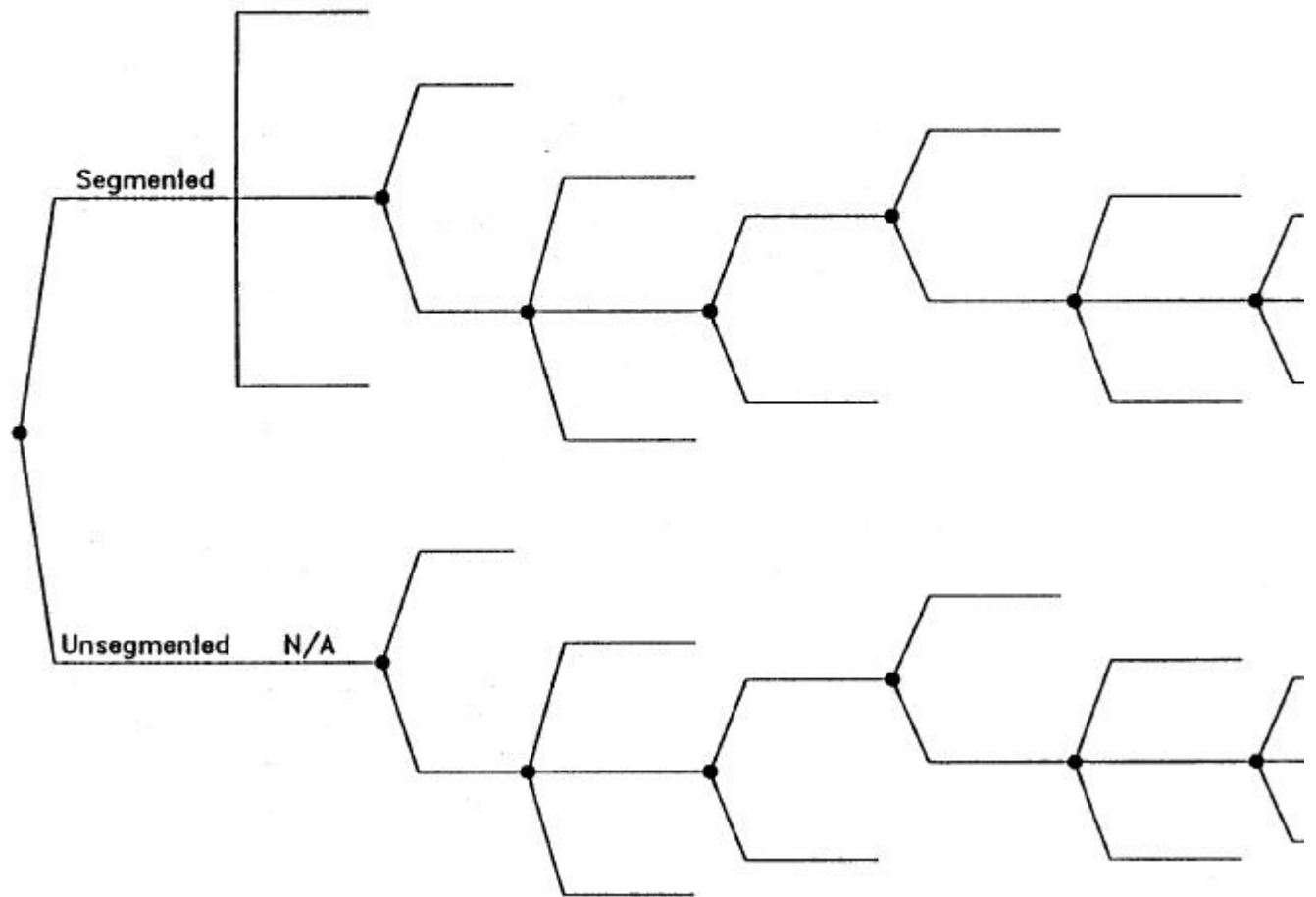
### c. Site in Illinois

(1) Seismic Source Characterization. The site location is shown in Figure E-23 and is in southern Illinois on the Ohio River. The dominant source zone for this site is the Iapetan Continental Rifts source zone (ICR), which represents an interconnected system of partially developed and failed continental rifts that lie within the mid-continent region of the United States and includes the New Madrid source zone (NSZ) where the large 1811 and 1812 earthquakes occurred. The extent of ICR is shown by the heavy line in Figure E-23 along with source zones outside ICR and the historical seismicity. Modeling of earthquake recurrence within the dominant ICR can be summarized as follows:

(a) The recurrence rate for large (1811-1812 type) earthquakes in NSZ is modeled based on paleoseismic evidence. As shown in Figure E-24, the paleoseismic-determined rate of these earthquakes exceed the rate of large earthquakes predicted from the historical seismicity.

(b) The recurrence rate for smaller earthquakes in ICR is determined by the historical seismicity. Two basic models are used within a logic tree framework for defining subzones for characterizing

<i>Segmentation</i>	<i>Segments</i>	<i>Total Length</i>	<i>Maximum Rupture Length</i>	<i>Maximum Magnitude Approach</i>	<i>Recurrence Approach</i>	<i>Slip/Activity Rates</i>	<i>b-</i>
---------------------	-----------------	---------------------	-------------------------------	-----------------------------------	----------------------------	----------------------------	-----------



E-20

Figure E-15 Generic logic tree used to characterize seismic sources for probabilistic seismic hazard analysis.

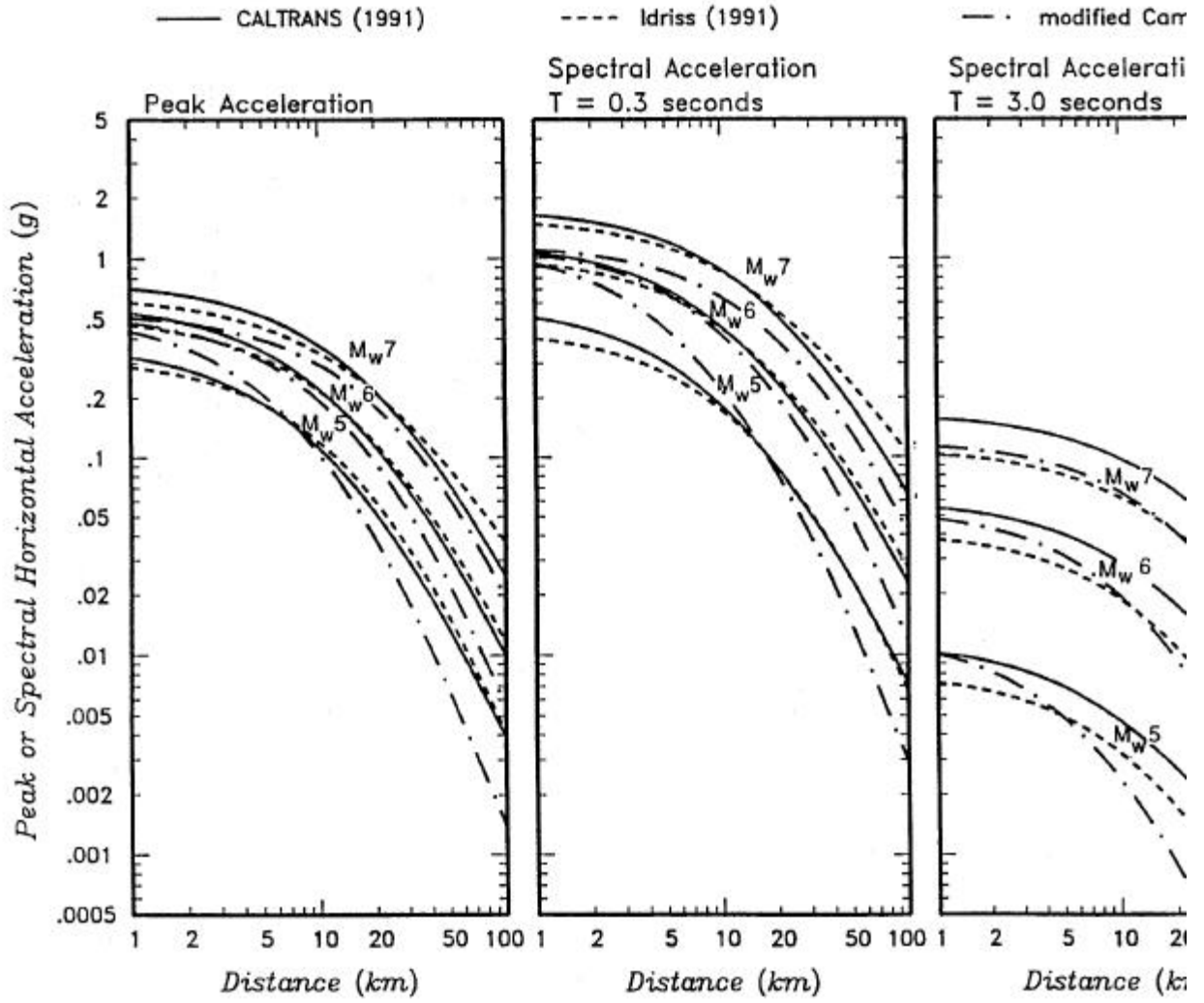


Figure E-16 Ground motion attenuation relationships.

Table E-1 Dispersion relationships for horizontal rock motion from the attenuation relationships of Sadigh et al. (1993).

<b>Ground Motion Parameter</b>	<b>Period</b>	<b>Sigma [ln(y)]</b>
Peak Ground Acceleration	--	1.39 - 0.14*M; 0.38 for M ≥ 7.21
Response Spectra Acceleration	0.05	1.39 - 0.14*M; 0.38 for M ≥ 7.21
Response Spectra Acceleration	0.07	1.40 - 0.14*M; 0.39 for M ≥ 7.21
Response Spectra Acceleration	0.09	1.40 - 0.14*M; 0.39 for M ≥ 7.21
Response Spectra Acceleration	0.10	1.41 - 0.14*M; 0.40 for M ≥ 7.21
Response Spectra Acceleration	0.12	1.41 - 0.14*M; 0.40 for M ≥ 7.21
Response Spectra Acceleration	0.14	1.42 - 0.14*M; 0.41 for M ≥ 7.21
Response Spectra Acceleration	0.15	1.42 - 0.14*M; 0.41 for M ≥ 7.21
Response Spectra Acceleration	0.17	1.42 - 0.14*M; 0.41 for M ≥ 7.21
Response Spectra Acceleration	0.20	1.43 - 0.14*M; 0.42 for M ≥ 7.21
Response Spectra Acceleration	0.24	1.44 - 0.14*M; 0.43 for M ≥ 7.21
Response Spectra Acceleration	0.30	1.45 - 0.14*M; 0.44 for M ≥ 7.21
Response Spectra Acceleration	0.40	1.48 - 0.14*M; 0.47 for M ≥ 7.21
Response Spectra Acceleration	0.50	1.50 - 0.14*M; 0.49 for M ≥ 7.21
Response Spectra Acceleration	0.75	1.52 - 0.14*M; 0.51 for M ≥ 7.21
Response Spectra Acceleration	1.00	1.53 - 0.14*M; 0.52 for M ≥ 7.21
Response Spectra Acceleration	>1.00	1.53 - 0.14*M; 0.52 for M ≥ 7.21

Note: Sigma [ln(y)] is the standard deviation of the natural logarithm of the respective ground motion parameter, y. M is the earthquake moment magnitude.

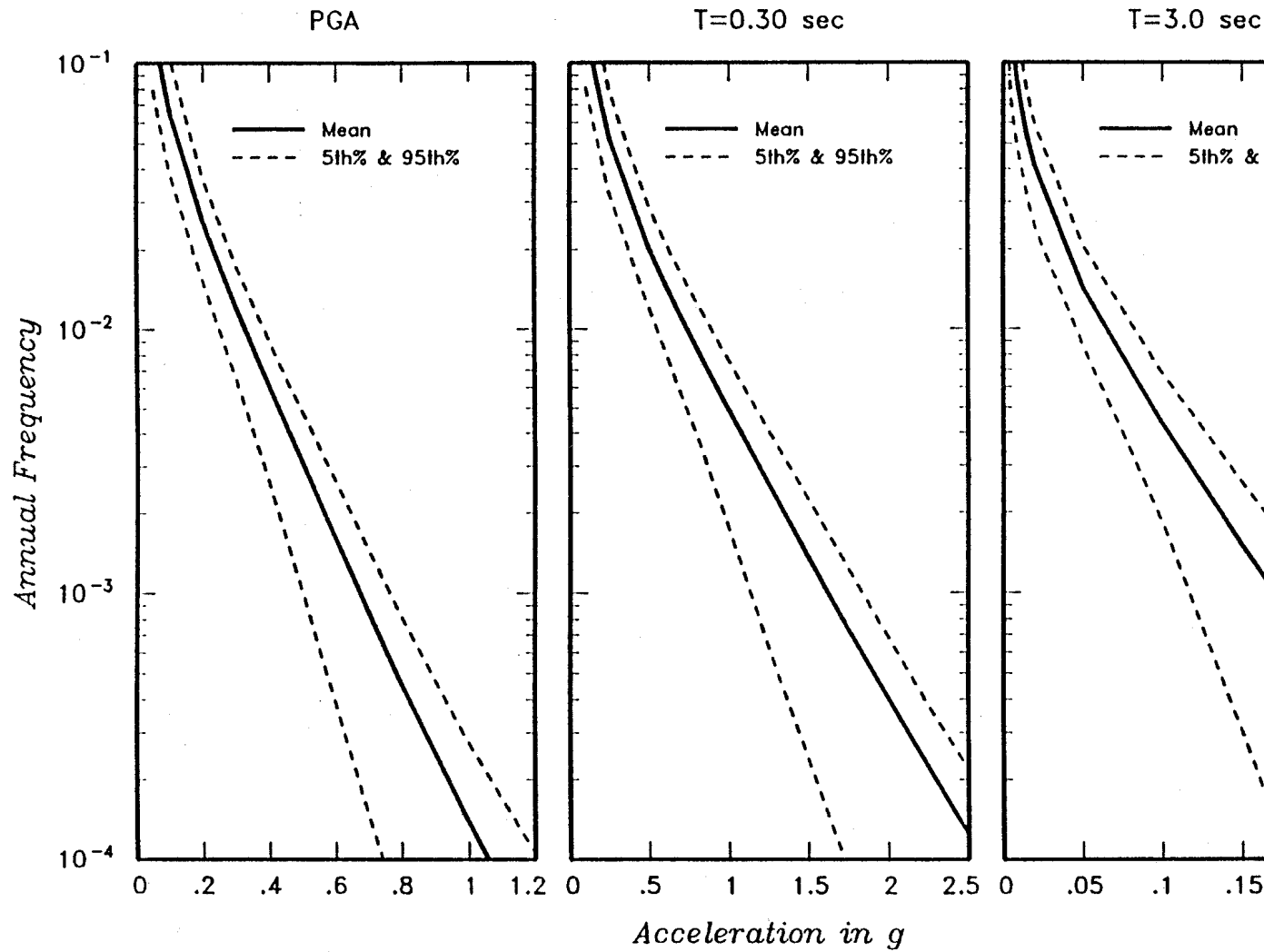


Figure E-17 Mean, 5<sup>th</sup>, and 95<sup>th</sup> percentile hazard curves for the site for peak acceleration and 5 percent accelerations at periods of 0.3 and 3.0 seconds.

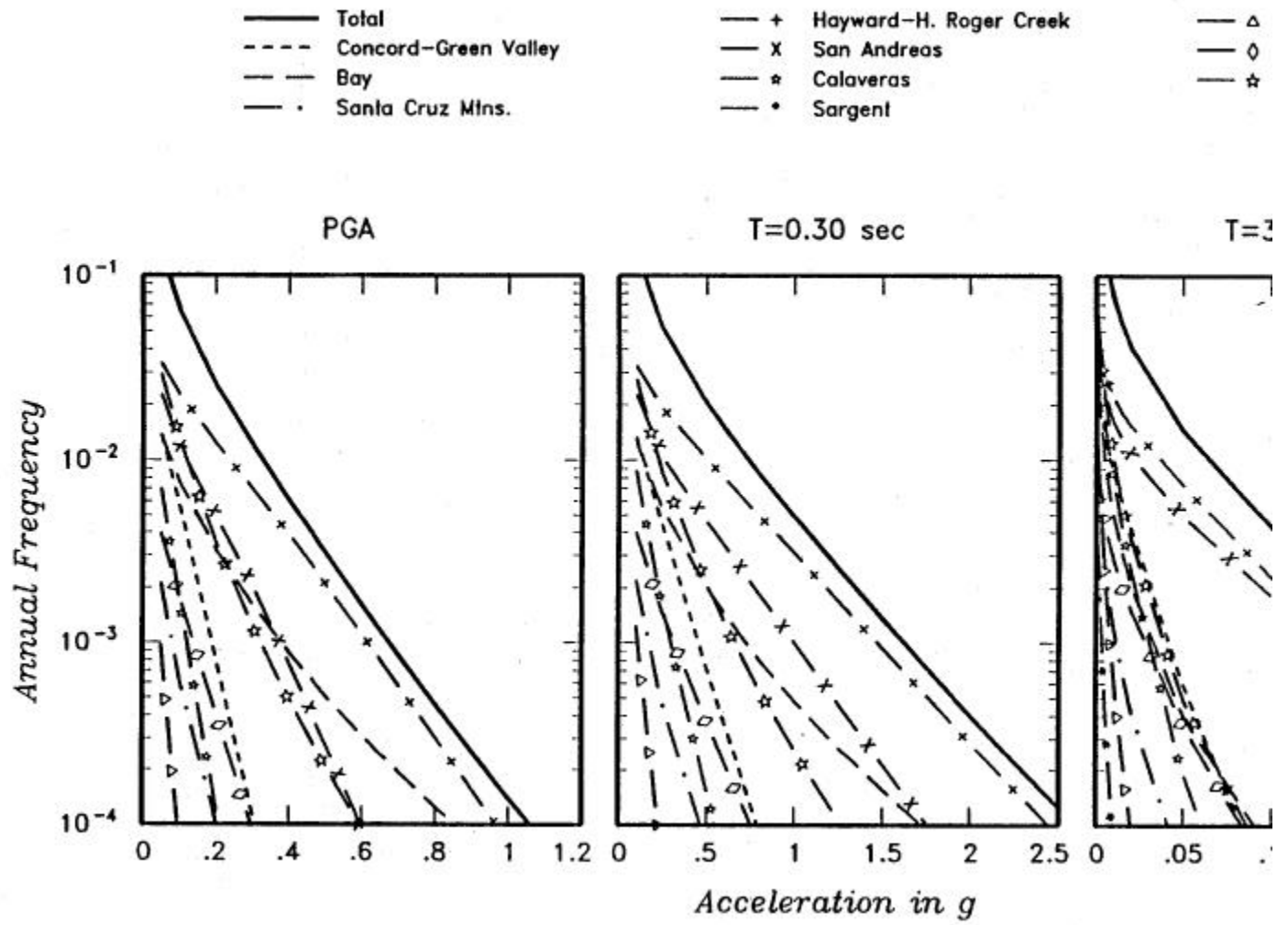


Figure E-18 Contributions of various sources to mean hazard at the site.

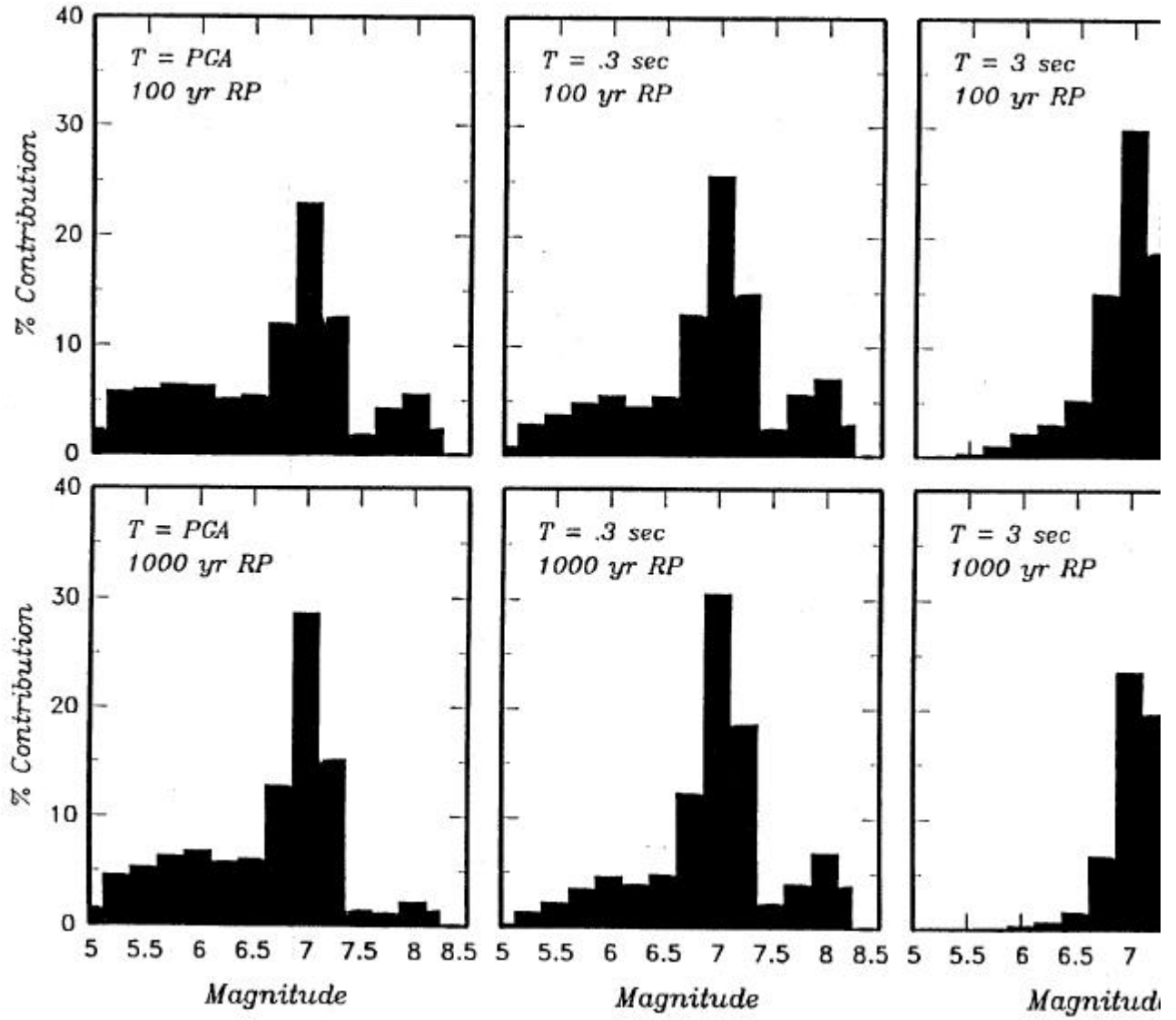


Figure E-19 Contributions of events in various magnitude intervals to the mean hazard at the site.

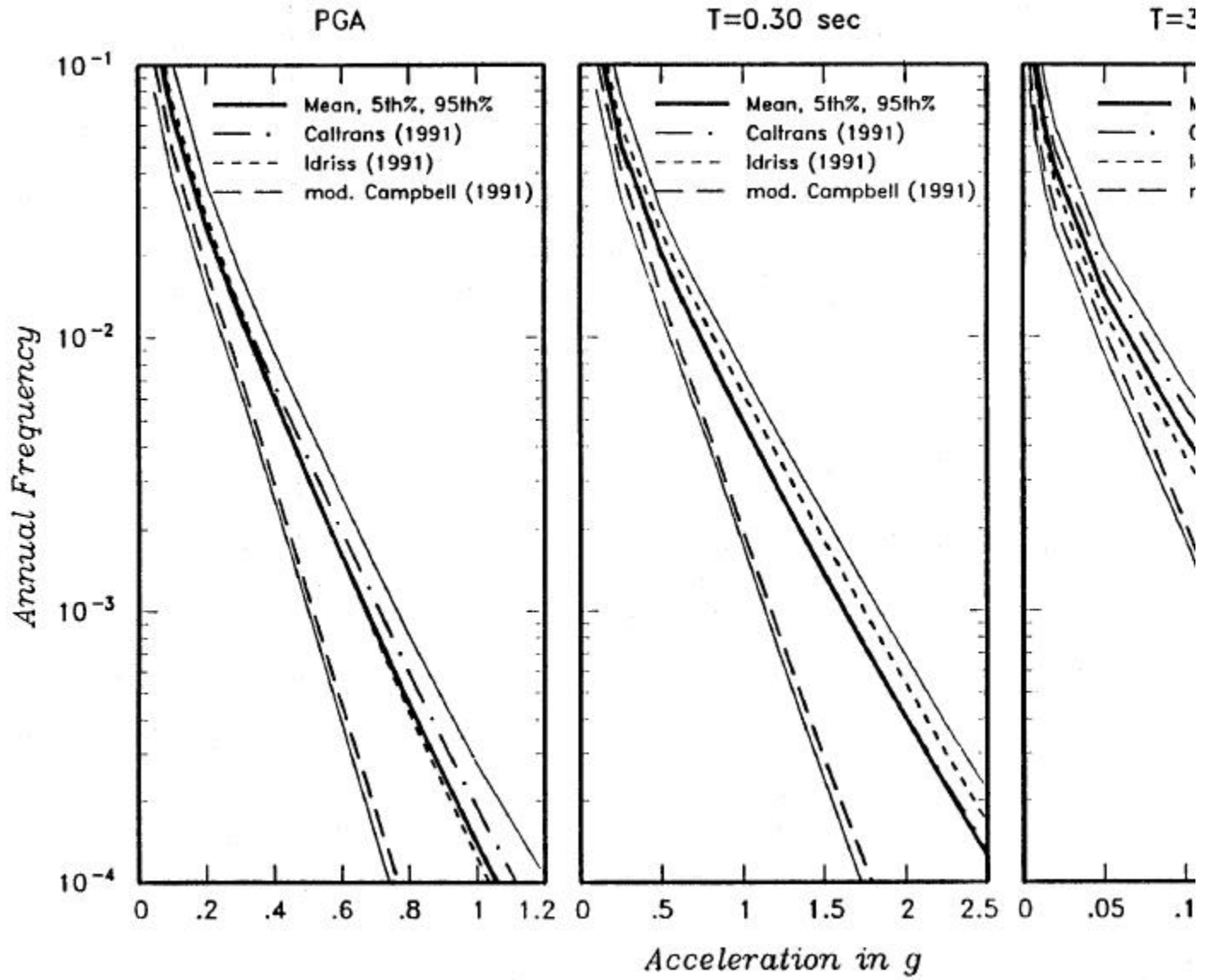


Figure E-20 Sensitivity of mean hazard at the site from the choice of attenuation model.

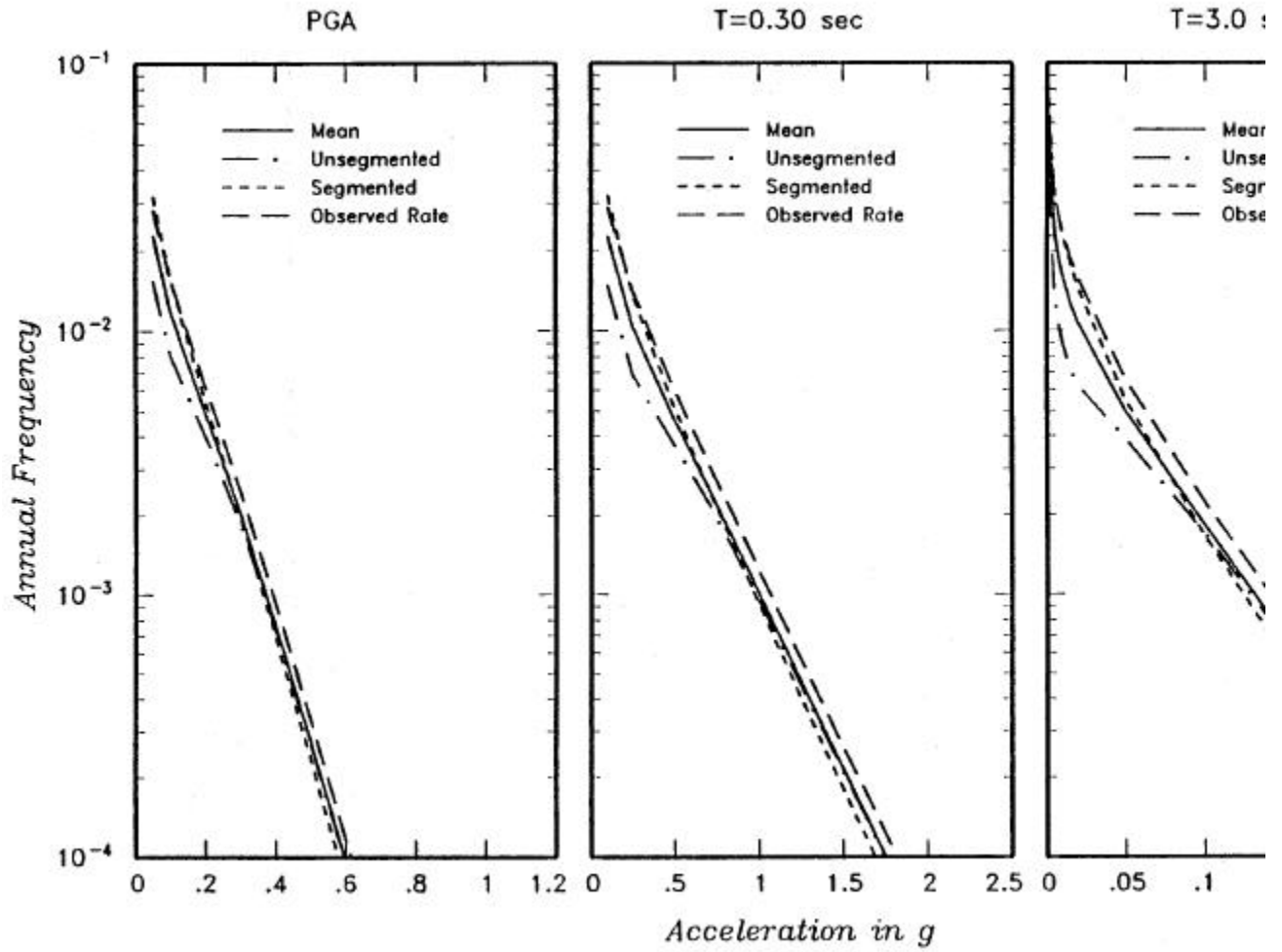


Figure E-21 Sensitivity of mean hazard at the site from the San Andreas fault only due to choice of earthquake model for the San Andreas fault.

- 2000-year Return Period
  - - - 1000-year Return Period
  - · - 500-year Return Period
  - · · 300-year Return Period
  - + 100-year Return Period
- (5% Damping)

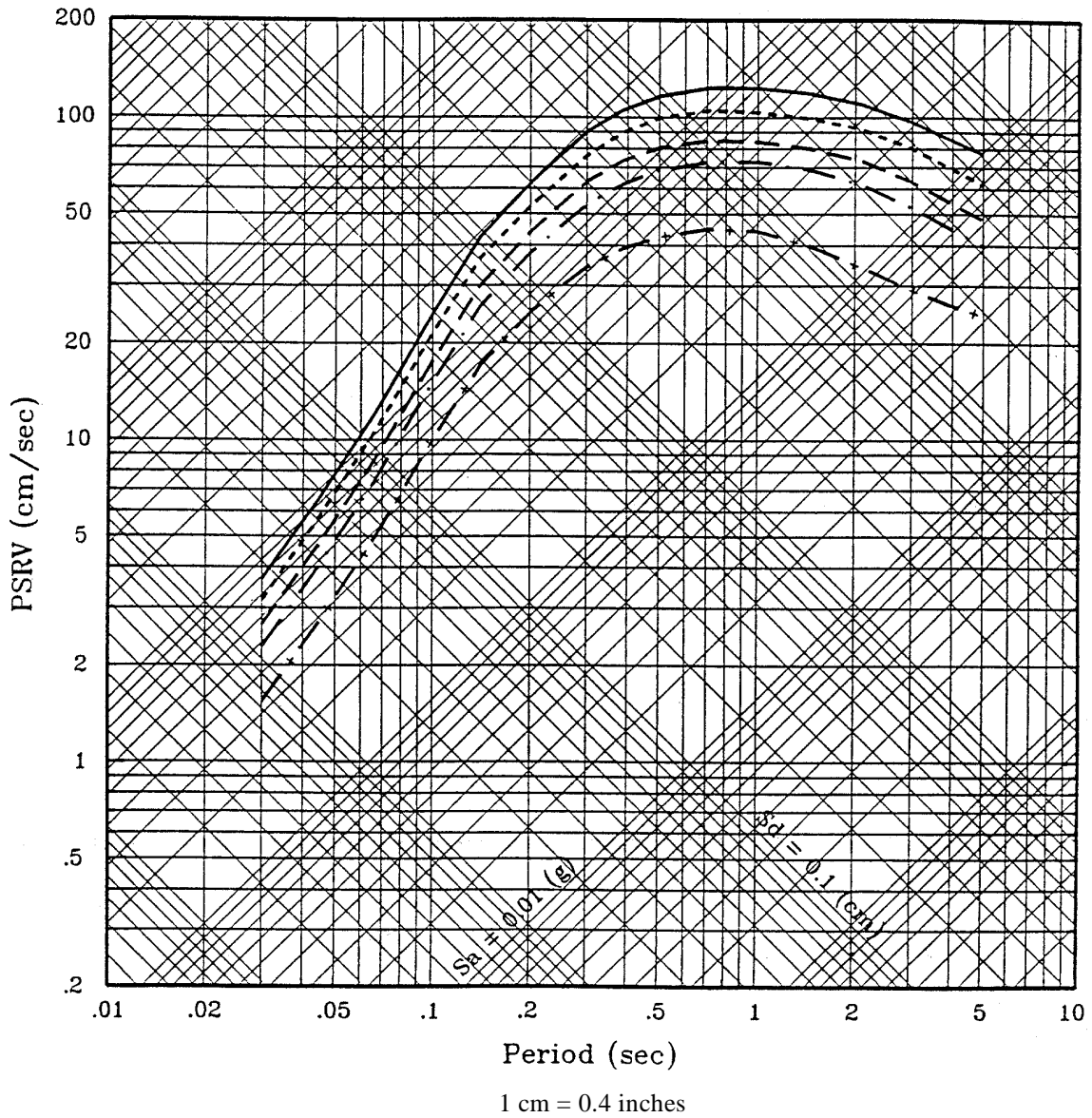


Figure E-22 Equal-hazard pseudo-velocity response spectra for the site (5 percent damping).

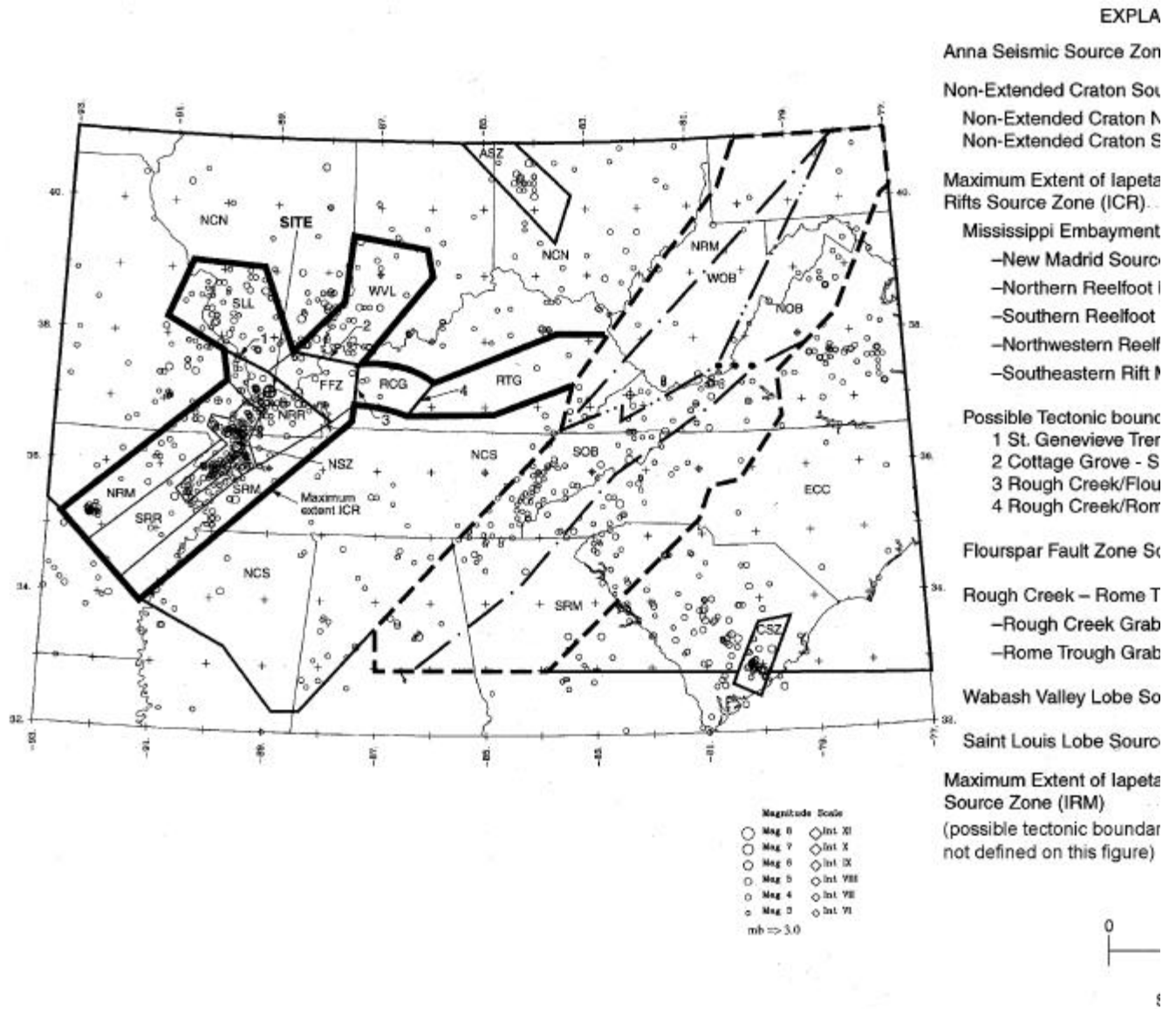


Figure E-23 Seismic source zonation model for the central and southeastern United States.

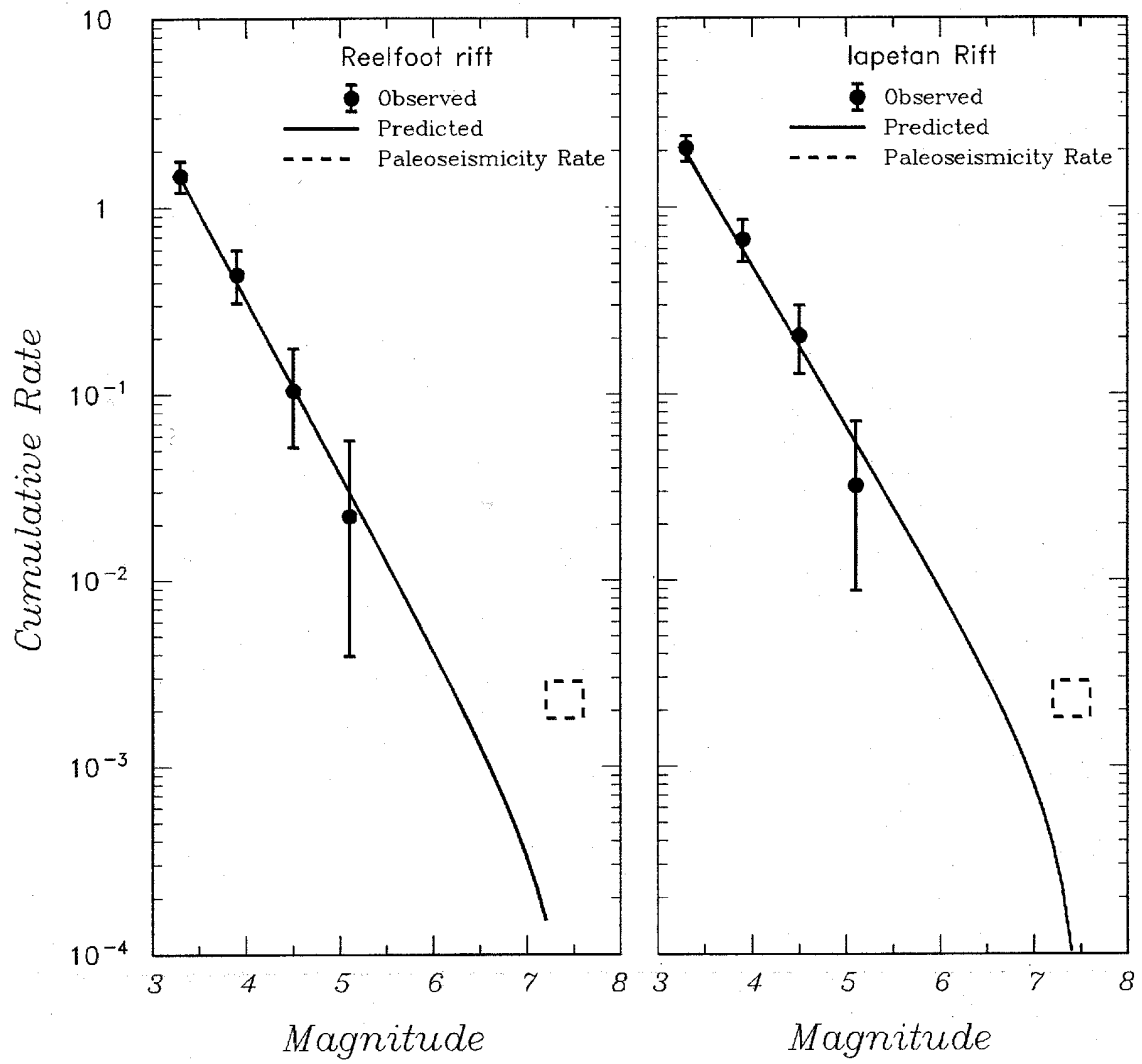


Figure E-24 Comparison of historical and paleoseismic recurrence estimates for the Reelfoot Rift and Iapetan Rift Seismic Zone.

recurrence within ICR: a seismicity-based model (given a weight of 0.25); and a geology-based model (given a weight of 0.75). The seismicity-based model divides ICR into cells of one-half degree latitude and longitude and calculates recurrence rates based on the historical seismicity in the cell. Different degrees of smoothing of seismicity rates and b-values among adjacent cells is accomplished using the methodology developed by EPRI (1988). In the geology-based model, Zone ICR is divided into subzones as indicated in Figure E-23. Different combinations of subzones are defined in a logic tree approach. The possible combinations are controlled in part by the presence or absence of four possible tectonic boundaries within the ICR (Figure E-23) and the assessed likelihood that these features represent fundamental boundaries that control the distribution, rate, and maximum magnitudes of seismicity. The logic tree for weights assigned to these boundaries is shown on Figure E-25. Thirty alternative subzonations (not shown herein) of ICR result from the logic tree of Figure E-25. Within each subzone of each alternative, seismicity rates are determined based on the seismicity within the subzone and assuming the rate is uniform within the subzone.

(c) Probabilistic distributions of maximum earthquake magnitudes are also part of the source model logic tree. These probabilistic distributions were determined using the methodology developed by EPRI (Johnston et al., 1994) that utilized worldwide data bases to assess maximum earthquake magnitudes in stable continental regions (like the eastern United States (EUS)) where active faults have not been identified and therefore maximum magnitude cannot be estimated on the basis of fault dimensions (as is done in the western United States (WUS)). However, for the New Madrid zone, maximum earthquake magnitudes were estimated on the basis of both (1) estimated rupture models by Johnston (1996) and Gomberg and Ellis (1994) and correlations of magnitude with rupture dimensions, and (2) estimates of magnitudes of the 1811-1812 earthquakes by Johnston (1996).

#### (2) Ground Motion Attenuation Characterization.

(a) It was desired to estimate ground motions on rock at the site. Two attenuation relationships applicable to hard rock in the EUS for horizontal peak ground acceleration and response spectral accelerations of ground motions at different periods of vibration were used. The relationships are those of EPRI (1993), (later published as Toro et al., 1997) and Atkinson and Boore (1995) (later published as Atkinson and Boore, 1997).

(b) The relationship for response spectral acceleration of EPRI (1993) extends to periods as long as

1 second, and that of Atkinson and Boore extends to a period of 2 seconds. The EPRI (1993) relationship was extrapolated to a period of 2 seconds. This was accomplished by extrapolating the coefficients of the attenuation relationship and examining the reasonableness of the resulting spectral prediction. The smooth quadratic form of the relationship of Atkinson and Boore (1995) underestimates their simulations of longer period ground motions at distances beyond 100 km (62 miles). Therefore, their relationships were modified at periods greater than 0.5 second to result in ground motion estimates closer to the simulation results. Plots of the attenuation relationships of EPRI (1993) and Atkinson and Boore (1995) for peak ground acceleration and response spectral accelerations at 1.0 second are presented in Figure E-26. The modifications to the 1-second motion at distances greater than 100 km (62 miles) can be seen in the figure. The plots in Figure E-26 clearly indicate the distinctive differences between the two eastern United States attenuation relationships: the Atkinson and Boore (1995) relationships result in higher spectral values than those of EPRI (1993) for peak ground acceleration and for short-period response spectral accelerations (less than about 0.2 second period), but lower values than those of EPRI (1993) at longer periods.

(c) In the hazard analysis, the relationship of EPRI (1993) was given a higher weight (0.67) than that of Atkinson and Boore (1995) (0.33). The reason for this judgment was that the EPRI (1993) relationship resulted from an EPRI study that involved input from a number of ground motion experts and thus could be viewed as having achieved a certain degree of consensus regarding the model. The practical effect of higher weighting on the EPRI (1993) model is to increase longer period ground motions and reduce short-period ground motions.

(3) PSHA Results. Hazard curves obtained from the analysis for peak ground acceleration and response spectral acceleration at two periods of vibration are shown in Figure E-27. The uncertainty bands around the mean curves, reflecting the alternative seismic source models and attenuation relationships incorporated into the logic tree, are shown in the figure. The contributions to the hazard are almost entirely from Zone ICR. Figure E-28 shows contributions within ICR from large New Madrid Zone earthquakes with rates defined by paleoseismic data (dashed-dotted line) and smaller earthquakes defined by seismicity (dashed line). It can be seen that the smaller earthquakes dominate hazard at higher frequencies (probabilities) of exceedance and the larger, 1811-1812-type earthquakes dominate at lower frequencies (probabilities) of exceedance. Figure E-29 compares the hazard obtained from geology-based and seismicity-based

<i>Ste. Genevieve Boundary</i>	<i>Cottage Grove Boundary</i>	<i>Rough Creek Boundary</i>	<i>Rome Trough Boundary</i>	<i>NSZ Present</i>	<i>Reelfoot Margin</i>
------------------------------------	-----------------------------------	---------------------------------	---------------------------------	------------------------	----------------------------

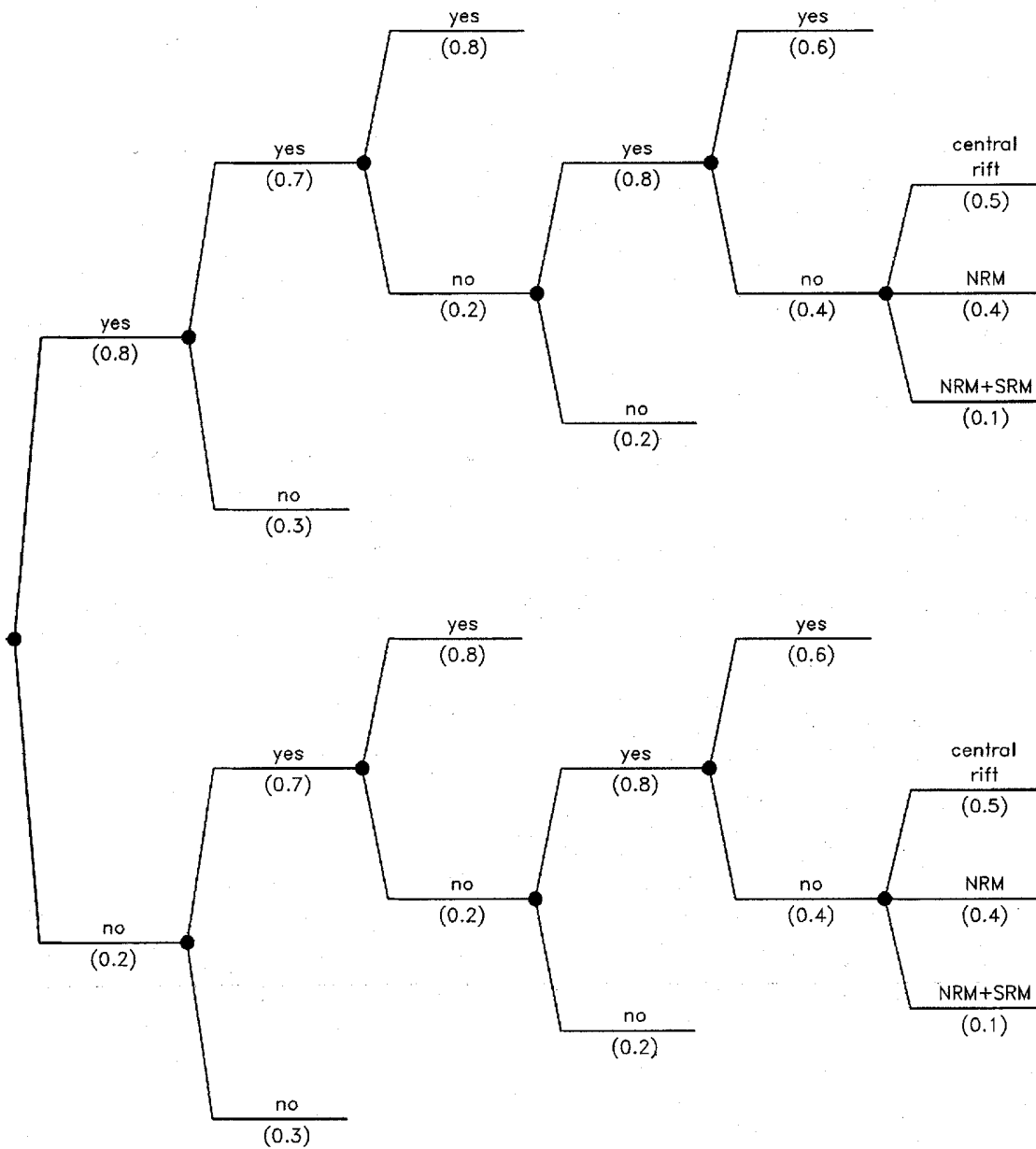


Figure E-25 Logic tree showing relative weights assigned to boundaries separating potential subzones of the Iapetan Rift Seismic Zone.

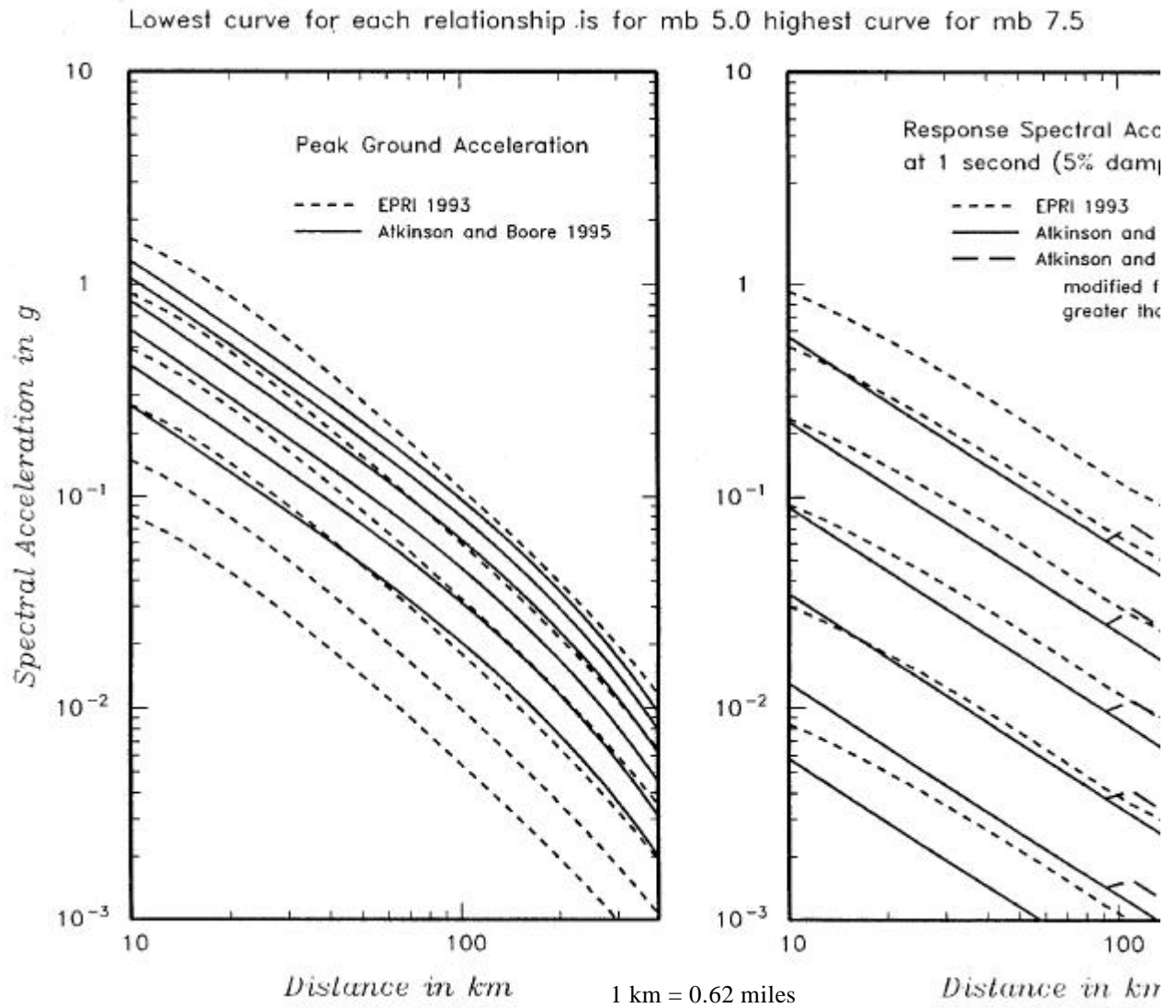


Figure E-26 Attenuation curves of Atkinson and Boore (1995) and EPRI (1993) for peak ground acceleration at 1.0 second period.

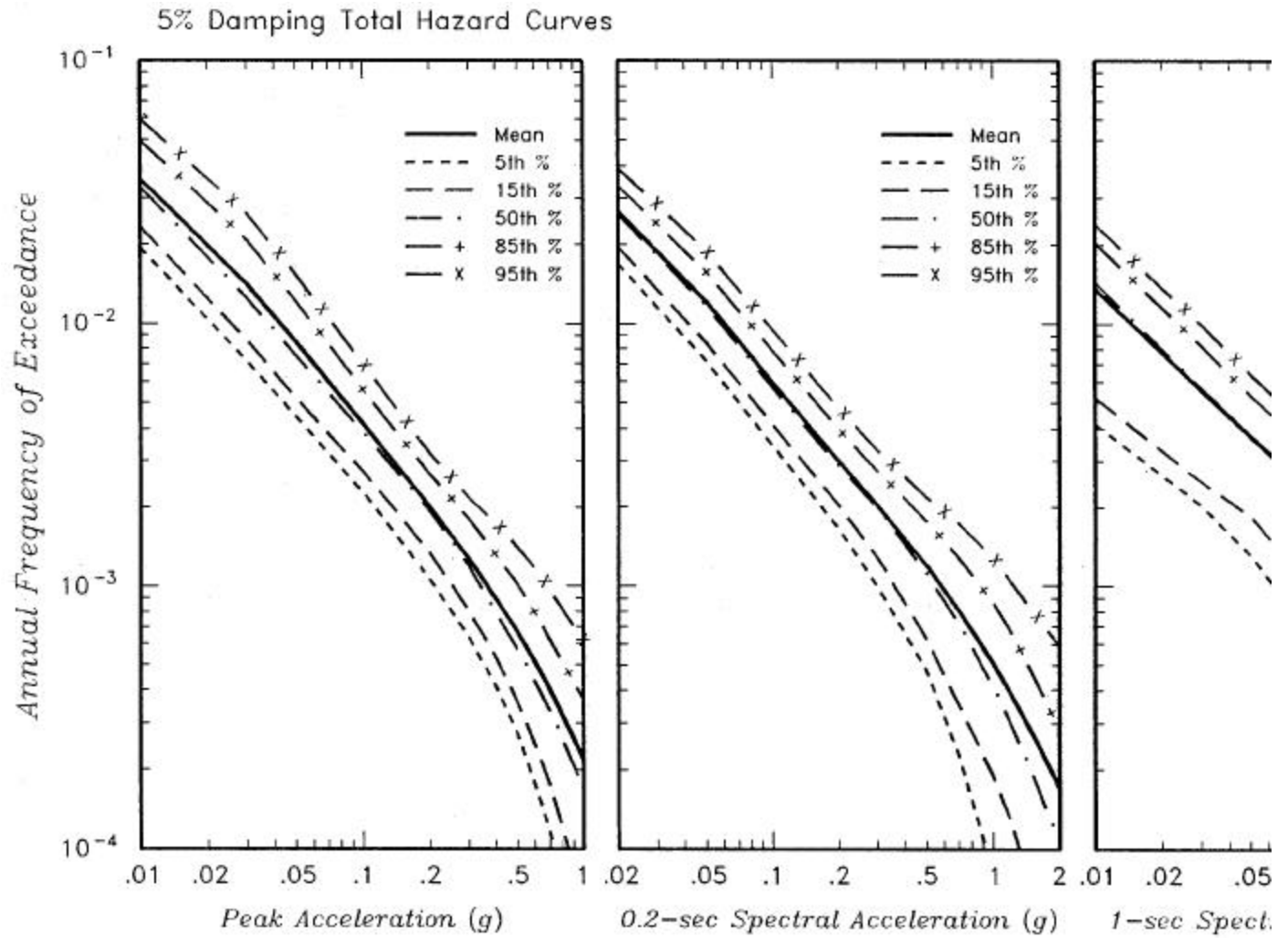


Figure E-27 Computed hazard for peak ground acceleration and response spectral accelerations at 0.2 and

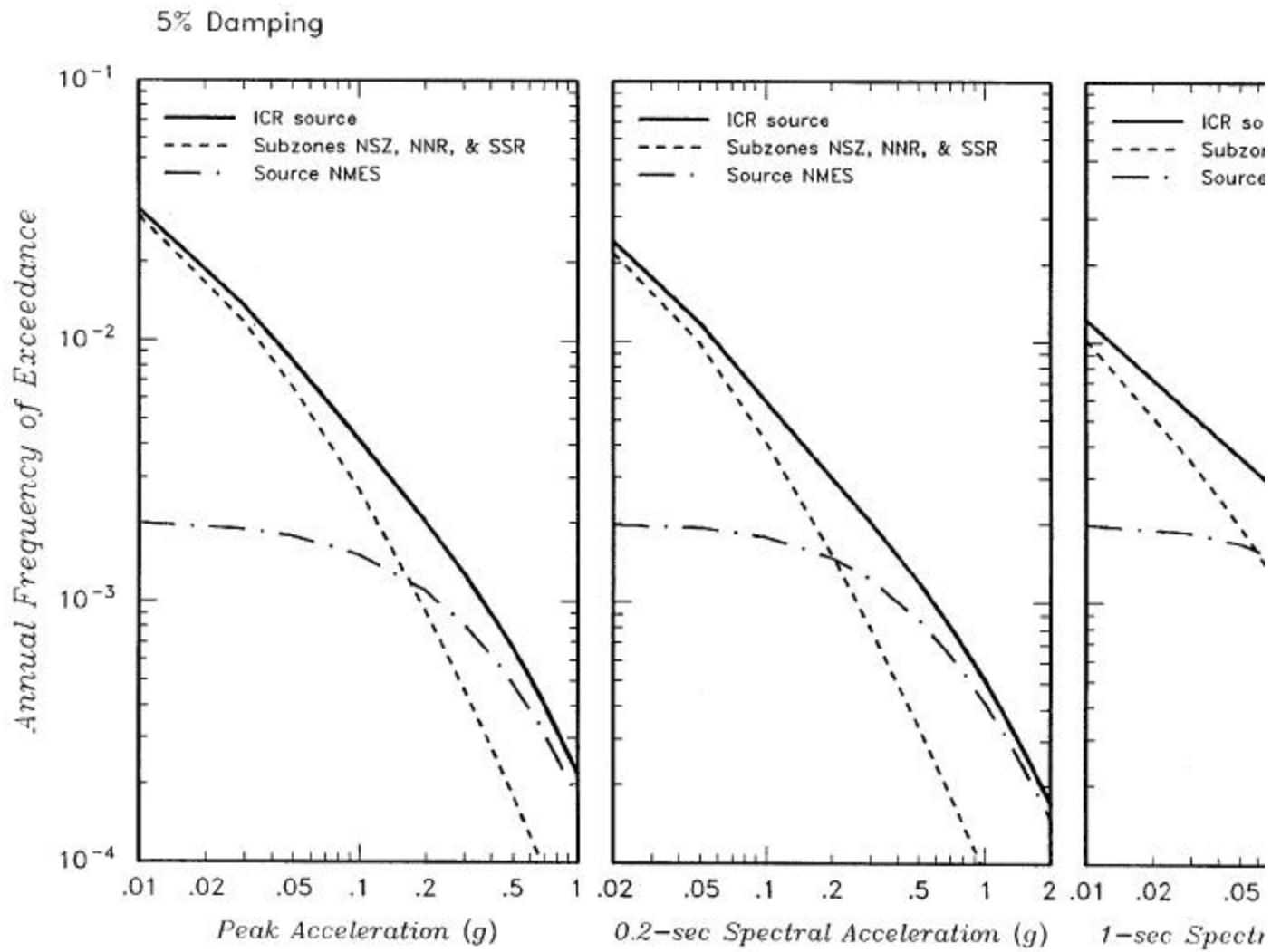


Figure E-28 Contributions of components of the ICR source to the hazard.

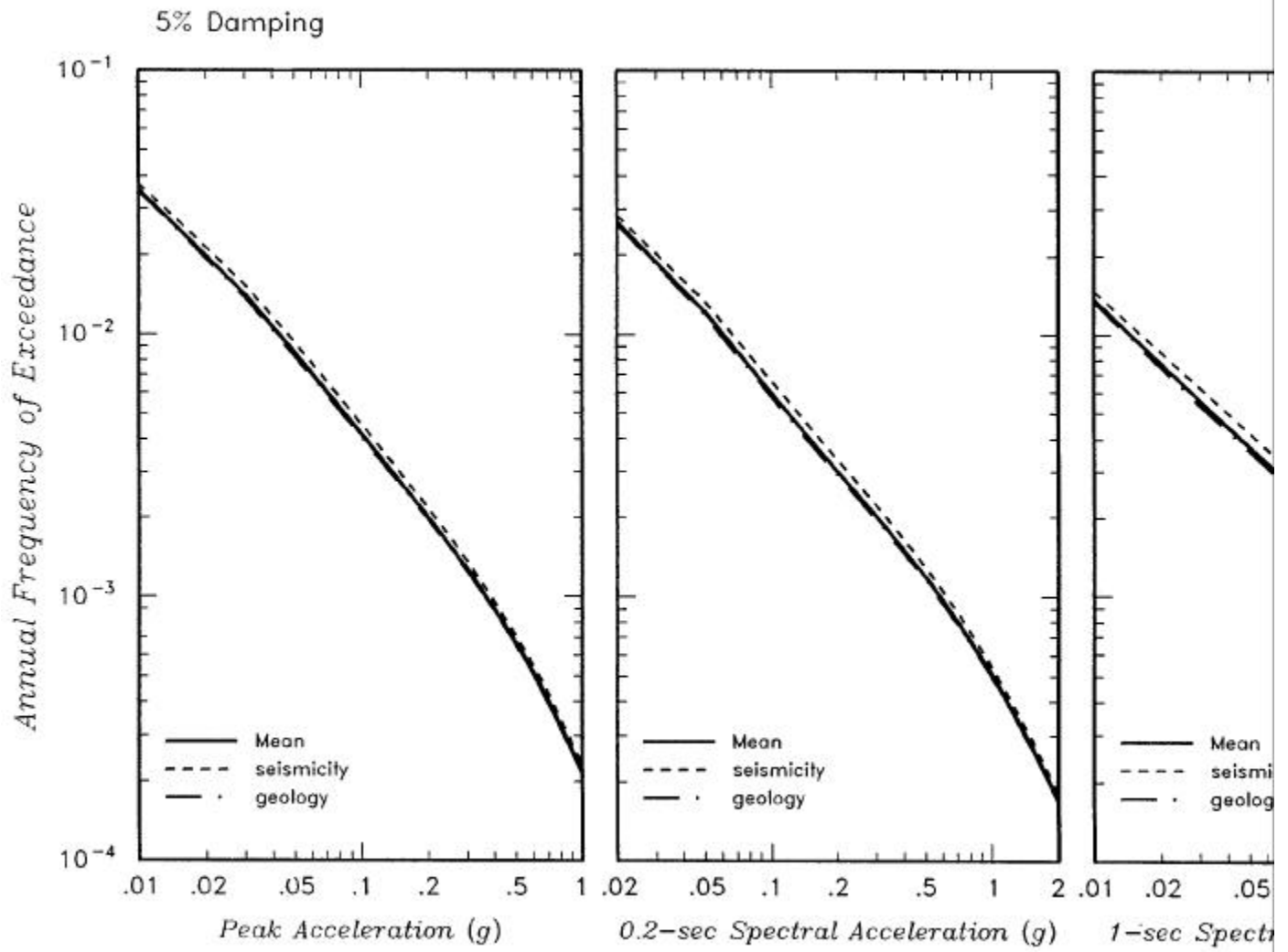


Figure E-29 Comparisons of hazard from the geology and seismicity-based models.

models. It can be seen that, for this site, the two modeling approaches lead to almost identical results. Equal-hazard response spectra obtained from the mean hazard results for all the periods of vibration analyzed for are shown in Figure E-30 for return periods varying from 144 to 10,000 years.

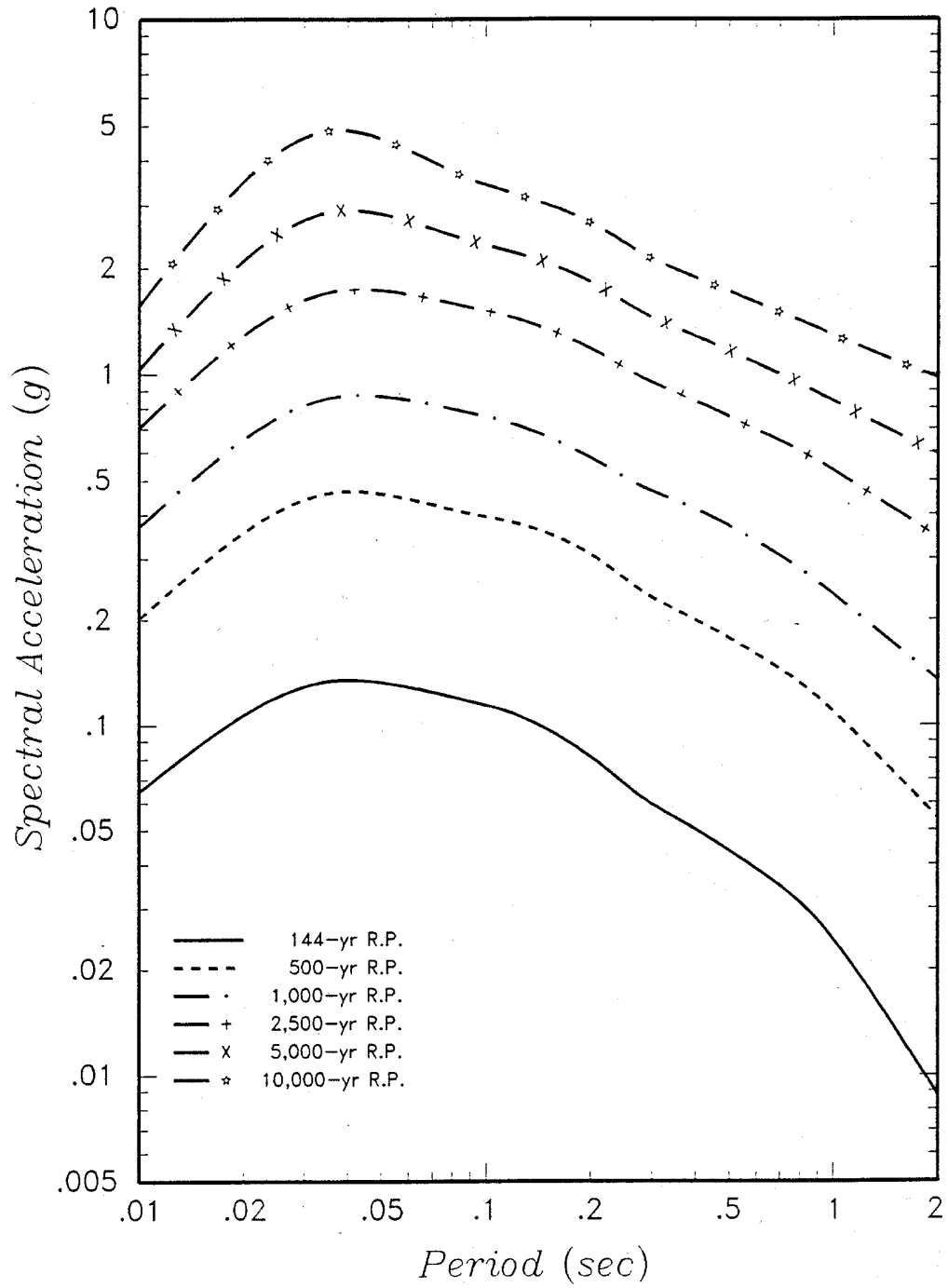


Figure E-30 Equal hazard response spectra (5% damping).